

ESTIMATION OF DYNAMIC SOIL PROPERTIES AND SOIL
AMPLIFICATION RATIOS WITH ALTERNATIVE TECHNIQUES

A THESIS SUBMITTED TO
THE GRADUATE SCHOOL OF NATURAL AND APPLIED SCIENCES
OF
MIDDLE EAST TECHNICAL UNIVERSITY

BY

FATMA NURTEN ŞİŞMAN

IN PARTIAL FULFILLMENT OF THE REQUIREMENTS
FOR
THE DEGREE OF THE MASTER OF SCIENCE
IN
EARTHQUAKE STUDIES

JANUARY 2013

Approval of the thesis:

**ESTIMATION OF DYNAMIC SOIL PROPERTIES AND SOIL AMPLIFICATION RATIOS
WITH ALTERNATIVE TECHNIQUES**

submitted by **FATMA NURTEN ŞİŞMAN** in partial fulfillment of the requirements for the degree of **Master of Science in Earthquake Studies Department, Middle East Technical University** by,

Prof.Dr. Canan Özgen
Dean, Graduate School of **Natural and Applied Sciences**

Prof.Dr. Melih Ersoy
Head of Department, **City and Regional Planning**

Assoc. Prof. Dr. Ayşegül Askan Gündoğan
Supervisor, **Civil Engineering Dept., METU**

Assist. Prof. Dr. Atilla Arda Özacar
Co-Supervisor, **Geological Engineering Dept., METU**

Examining Committee Members:

Prof. Dr. M.Semih Yücemem
Civil Engineering Dept., METU

Assoc. Prof. Dr. Ayşegül Askan Gündoğan
Civil Engineering Dept., METU

Assist. Prof. Dr. Atilla Arda Özacar
Geological Engineering Dept., METU

Assist. Prof. Dr. Zeynep Gülerce
Civil Engineering Dept., METU

M.Sc. Tuğbay Kılıç
Disaster and Emergency Management Presidency

Date:

29.01.2013

I hereby declare that all information in this document has been obtained and presented in accordance with academic rules and ethical conduct. I also declare that, as required by these rules and conduct, I have fully cited and referenced all material and results that are not original to this work.

Name, Last name : Fatma Nurten, ŞİŞMAN

Signature :

ABSTRACT

ESTIMATION OF DYNAMIC SOIL PROPERTIES AND SOIL AMPLIFICATION RATIOS WITH ALTERNATIVE TECHNIQUES

Şişman, Fatma Nurten
M.Sc., Department of Earthquake Studies
Supervisor: Assoc. Prof. Dr. Ayşegül Askan Gündoğan
Co-Supervisor: Assist. Prof. Dr. Atilla Arda Özacar

January 2013, 71 pages

Earthquakes are among the most destructive natural disasters affecting urban populations. Structural damage caused by the earthquakes varies depending not only on the seismic source and propagation properties but also on the soil properties. The amplitude and frequency content of seismic shear waves reaching the earth's surface is dependent on local soil conditions. It is well known that the soft sediments on top of hard bedrock can greatly amplify the ground motion and cause severe structural damage. When the fundamental period of the soil is close to the fundamental period of a structure, structural damage increases significantly. Estimation of the fundamental periods, amplification factors and types of soils is critical in terms of reduction of loss and casualties. For the reasons stated, estimation of dynamic behavior of soils has become one of the major topics of earthquake engineering. Studies for determining dynamic properties of soils depend fundamentally on the estimation of the S-wave velocity profiles, amplification factors and ground response.

In this study first, the Multi-Mode Spatial Autocorrelation (MMSPAC) method is used to estimate the S-wave velocity profiles at the sites of interest. This method is different than the other ones in the sense that it works for the higher modes as well as the fundamental mode. In the second part, Horizontal to Vertical Spectral Ratio (HVSr) method will be used on both microtremor and ground motion data. Finally, the amplification factors from alternative methods are compared with each other. Consistent results are obtained in terms of both fundamental frequencies and amplification factors.

Keywords: Microtremors, surface waves, MMSPAC method, S-wave velocity, dynamics of soil properties, soil amplification

ÖZ

ZEMİNLERİN DİNAMİK ÖZELLİKLERİNİN VE ZEMİN BÜYÜTME FAKTÖRLERİNİN ALTERNATİF YÖNTEMLERLE BELİRLENMESİ

Şişman, Fatma Nurten
Yüksek Lisans, Deprem Çalışmaları Bölümü
Tez Yöneticisi: Doç. Dr. Ayşegül Askan Gündoğan
Yardımcı Tez Yöneticisi: Yard. Doç. Dr. Atilla Arda Özacar

Ocak 2013, 71 sayfa

Depremler, kentsel alanları etkileyen en tahrip edici doğal afetlerdendir. Depremlerin oluşturduğu yapı hasarları, depremin yalnızca odak ve yayılım özelliklerine değil, zemin özelliklerine bağlı olarak da büyük farklılıklar göstermektedir. Yeryüzüne ulaşan sismik kesme (kayma) dalgalarının genlik ve frekans içerikleri, lokal zemin koşullarına bağlıdır. Sert anakayanın üzerinde yer alan yumuşak zeminlerin yer hareketini büyüterek ağır yapı hasarlarına neden olabildiği bilinmektedir. Zemin hakim periyodu, yapının hakim periyoduna yakın olduğunda, yapısal hasar önemli ölçüde artmaktadır. Hakim periyot, büyütme faktörü ve zemin tipi değerlendirmeleri, can ve mal kaybını azaltma açısından oldukça kritik bir husustur. Belirtilen nedenlerden ötürü, zemin dinamik davranışlarının değerlendirilmesi deprem mühendisliği için temel konulardan birisi haline gelmiştir. Zeminlerin dinamik özelliklerini belirleme çalışmaları, temel olarak S-dalgası hız profili, büyütme faktörü ve zemin tepkisi elde etmeye dayanır.

Bu çalışmada ilk olarak, Çoklu-mod Uzaysal Özilişki metodu kullanılarak ilgili sahalarda S-dalga hız profili değerlendirilmesi yapılmıştır. Bu metod, temel modların yanısıra yüksek modlar için de başarıyla kullanılabilmesi açısından diğerlerinden farklılık gösterir. İkinci aşamada, Yatay/Düşey Spektral Oran metodu, hem mikrotremor verileri hem de yer hareketi verileri üzerinde uygulanmıştır. Son olarak, alternatif metotlardan elde edilen büyütme faktörleri birbirleriyle karşılaştırılmıştır. Hakim frekans ve zemin büyütme faktörü açısından birbiri ile uyumlu sonuçlar elde edilmiştir.

Anahtar Kelimeler: Mikrotremor, yüzey dalgaları, MMSPAC yöntemi, S-dalga hızı, zeminlerin dinamik özellikleri, zemin büyütmesi

*To My Parents and My Fiance
to My Supervisor Assoc. Prof. Dr. Aysegül Askan Gündođan*

ACKNOWLEDGMENTS

I would like to express my deepest gratitude to my supervisor, Assoc. Prof. Dr. Ayşegül Askan Gündoğan for her invaluable guidance, knowledge, support, encouragement and insight throughout the research and is grateful for the opportunity to work with her.

I would like to thank Prof. Dr. Michael Asten for his patience and support and for sharing his knowledge endlessly. I am also grateful to Inst. Dr. Onur Pekcan for sharing his knowledge and support during my graduate studies.

I have been supported by the Scientific and Technological Research Council of Turkey (TÜBİTAK-109M390), European Union (Network of European Research Infrastructures for Earthquake Risk Assessment and Mitigation (NERA)) and Turkish National Geodesy and Geophysics Union (TUJJB-UDP-01-12) throughout this master period and I would like to acknowledge these supports.

I would like also to thank my dear family members, my mother Ayla Şişman, my father Mustafa Kemal Şişman, my sister Mesude Özlem Şişman and my fiance Ahmet Dersan for their love and support.

Finally, I would like to thank to my dear cousin Sibel Develi Boyacıoğlu, my roommate Betül Ozar, my officemates Arash Maghsoudloo and my friends Mustafa Bilal, Ezgi Ertürk, Ezgi Baksı, Görkem Yenim, Bahadır Kargioğlu and Gürkan Eraslan for their support, advice and friendship.

TABLE OF CONTENTS

ABSTRACT	v
ÖZ	vi
ACKNOWLEDGMENTS.....	viii
TABLE OF CONTENTS	ix
LIST OF TABLES.....	xi
LIST OF FIGURES.....	xii
CHAPTERS	
1. INTRODUCTION.....	1
1.1 General	1
1.2 Objectives and Scope.....	2
2. ESTIMATION OF ONE-DIMENSIONAL SHEAR WAVE VELOCITY PROFILES WITH MULTI-MODE SPATIAL AUTOCORRELATION METHOD (MMSPAC)	3
2.1 General	3
2.2 Microtremors (Microseism)	3
2.3 The Microtremor Survey Method (MSM)	4
2.4 Implementation of SPAC Method	4
2.4.1 Collection of SPAC Data and Properties of Array Geometry	5
2.4.2 Calculation of the SPAC Coefficient.....	6
2.4.3 Estimation of the Phase Velocity with Traditional SPAC Method for Near-Surface Structure.....	7
2.5 Implementation of MMSPAC Method	8
2.5.1 Collection of MMSPAC Data and Properties of Array Geometry.....	8
2.5.2 Pre- processing and Data Analyses in MMSPAC Method	9
2.6 Study Areas: Düzce and Bolu.....	13
2.6.1 Previous Microtremor and Surface-Wave Surveys in the Region.....	15
2.6.2 MMSPAC Array Data in Düzce and Bolu	19
2.6.3 Results from MMSPAC Interpretations for Düzce and Bolu	20
3. EVALUATION OF SITE RESPONSE BASED ON ALTERNATIVE METHODS.....	29
3.1 General	29
3.2 Horizontal to Vertical Spectral Ratio Method.....	29
3.2.1 HVSr Analyses of Microtremor Data	32
3.2.2 HVSr Analyses of Earthquake Data.....	33
3.3 One-Dimensional Site Response Modeling.....	38
3.3.1 Theory of One-Dimensional Site Response Analysis	38
3.3.2 Implementation of One-Dimensional Site Response Modeling.....	43

3.4	Comparison of Results from Alternative Techniques.....	45
4.	SUMMARY AND CONCLUSIONS	49
4.1	Summary	49
4.2	Conclusions.....	49
4.3	Future Work and Recommendations	51
	REFERENCES	53
	APPENDICES	
A.	ADDITIONAL CASE STUDIES	59
A.1	Wien 1 Data	59
A.2	Wien 2 Data	61
A.2.1	Results of the radius 10m	62
A.2.2	Results of the radius 20m	63
A.2.3	Results of the radius 40m	65
A.2.4	Results of the radius 80m	66
A.2.5	Results of the radius 160m	68
A.2.6	Results of the multiple solution (Radii 40m-80m and 160m).....	69

LIST OF TABLES

TABLES

Table 2.1: Information on the previous studies for determining S-wave velocity profiles in Düzce and Bolu	15
Table 2.2: Layered-earth model at Düzce site from combined SPAC and HVSR modelling	24
Table 2.3: Layered-earth model at Bolu site from combined SPAC and HVSR modeling ...	26
Table 3.1: Information on the ground motion records (with $PGA < 0.015$ g) recorded at station Düzce	35
Table 3.2: Information on the ground motion records (with $PGA < 0.015$ g) recorded at station Bolu	36
Table 3.3: Geotechnical and geophysical parameters of the soil layers at Düzce site.....	44
Table 3.4: Geotechnical and geophysical parameters of the soil layers at Bolu site.....	45
Table A.1: Layered-earth model at Wien 1 (Radius: 7m)	61
Table A.2: Layered-earth model at Wien 2 (Radius: 10m)	63
Table A.3: Layered-earth model at Wien 2 (Radius: 20m)	64
Table A.4: Layered-earth model at Wien 2 (Radius: 40m)	66
Table A.5: Layered-earth model at Wien 2 (Radius: 80m)	67
Table A.6: Layered-earth model at Wien 2 (Radius: 160m)	69
Table A.7: Layered-earth model at Wien 2 (multiple solutions)	70

LIST OF FIGURES

FIGURES

Figure 2.1: Main steps of traditional SPAC Implementations (Figure is adapted from Maresca et al., 2006).....	5
Figure 2.2: Array geometries for SPAC method used in literature. (a) and (b) demonstrate triangular arrays (c) is a hexagonal array, (d) is a square or a linear cross array, and (e) is a semi-circular array (Figure is adapted from Asten, 2004).	6
Figure 2.3: Circular layout for microtremor measurement with traditional SPAC method.....	7
Figure 2.4: Step by step description of a typical MMSPAC field work	10
Figure 2.5: Major steps of MMSPAC implementation	11
Figure 2.6: Flowchart for the computer implementation of MMSPAC method.....	12
Figure 2.7: Map demonstrates tectonic settings of Turkey. The dashed rectangle indicates the study areas and large arrows represent the direction of relative plate motions. (Figure is adapted from Utkucu et al., 2003).	13
Figure 2.8: Geological map of Düzce and Bolu (Grey areas are undifferentiated Quaternary at Düzce and Bolu. Stars indicate the location of the strong ground motion stations where the measurements are taken.) (Figure is adapted from www.mta.gov.tr)	14
Figure 2.9: Düzce site: S-wave profile obtained by Kudo (2002)	16
Figure 2.10: Düzce site: S-wave profile obtained by Yamanaka (2002)	16
Figure 2.11: Düzce site: S-wave profile obtained by Rosenblad (2006)	16
Figure 2.12: Düzce site: S-wave profile obtained by Yılmaz et al. (2008a)	17
Figure 2.13: Düzce site: S-wave profile obtained by Yılmaz et al. (2008b)	17
Figure 2.14: Düzce site: S-wave profile obtained by Yılmaz et al. (2008b)	17
Figure 2.15: Düzce site: S-wave profile obtained by Alexoudi (2008)	18
Figure 2.16: Bolu site: S-wave profile obtained by Tokgöz (2002)	18
Figure 2.17: Bolu site: S-wave profile obtained by Başokur (2005)	18
Figure 2.18: Bolu site: S-wave profile obtained by Rosenblad et al. (2006)	19
Figure 2.19: Bolu site: S-wave profile obtained by Ansal et al. (2007)	19
Figure 2.20: a) Guralp CMG6TD seismometer (Figure is adapted from http://www.guralp.com) b) Standard centered-triangular arrays c) Sketch map of arrays at Düzce Strong Ground Motion Station d) Sketch map of array at Bolu Strong Ground Motion Station.....	20
Figure 2.21: SPAC spectra at Düzce (small array) (Top Panel: SPAC spectra for r1, Bottom Panel: SPAC spectra for r2)	21
Figure 2.22: Dispersion curve at Düzce (small array) (Black curves indicate theoretical dispersion curves whereas the red dots indicate observed dispersion).....	22
Figure 2.23: SPAC spectra at Düzce (large array) (Top Panel: SPAC spectra for r1, Bottom Panel: SPAC spectra for r2)	22

Figure 2.24: Dispersion curve at Düzce (large array) (Black curves indicate theoretical dispersion curves whereas the red dots indicate observed dispersion)	23
Figure 2.25: S-wave velocity profile at Düzce.....	23
Figure 2.26: SPAC spectra at Bolu array (Top Panel: SPAC spectra for r1, Bottom Panel: SPAC spectra for r2).....	25
Figure 2.27: Dispersion curve at Bolu array (Black curves indicate theoretical dispersion curves whereas the red dots indicate observed dispersion).....	25
Figure 2.28: S-wave velocity profile at Bolu.....	26
Figure 2.29: Comparison of the S-wave velocity profile obtained in this thesis with previous studies at Düzce site.....	27
Figure 2.30: Comparison of the S-wave velocity profile obtained in this thesis with previous studies at Bolu site.....	27
Figure 3.1: Flow chart displaying the analyses used in this chapter.....	30
Figure 3.2: A typical four-station equilateral triangular array used for microtremor measurements in this study (A, B, C and G indicate the seismometer locations; r1 and r2 are the inter-station separations).....	32
Figure 3.3: HVSr from microtremors at Düzce	32
Figure 3.4: HVSr from microtremors at Bolu	33
Figure 3.5: Main steps of HVSr method with ground motion data.....	34
Figure 3.6: HVSr spectra from weak (a) and strong (b) ground motion at Düzce	37
Figure 3.7: HVSr spectra from weak (a) and strong (b) ground motion at Bolu	37
Figure 3.8: Refraction process (Figure is adapted from Kramer, 1996)	38
Figure 3.9: Description of terms used in analysis (Kramer, 1996).....	39
Figure 3.10: Illustration of a single layer of soil an elastic rock.....	39
Figure 3.11: Illustration of a layered soil deposit on elastic rock	41
Figure 3.12: Transfer function at Düzce.....	43
Figure 3.13: Transfer function at Bolu.....	44
Figure 3.14: Comparison of amplification spectra at Düzce in terms of (a) HVSr from microtremors, (b) HVSr from weak motions, (c) HVSr from 1999 Kocaeli and 1999 Düzce mainshocks, (d) Theoretical transfer functions	47
Figure 3.15: Comparison of amplification spectra at Bolu in terms of (a) HVSr from microtremors, (b) HVSr from weak motions, (c) HVSr from 1999 Kocaeli and 1999 Düzce mainshocks, (d) Theoretical transfer functions	48
Figure A.1: Sketch map of array measurements	59
Figure A.2: SPAC coherency curve at Wien 1	60
Figure A.3: Dispersion curve at Wien 1 (Black curves indicate theoretical dispersion curves whereas the red dots indicate observed dispersion)	60
Figure A.4: S-wave velocity profile at Wien 1 (Radius: 10m).....	60
Figure A.5: Sketch map of arrays at Wien	61
Figure A.6: SPAC coherency curve at Wien 2 for radius 10m.....	62
Figure A.7: Dispersion curve at Wien 2 for radius 10m (Black curves indicate theoretical dispersion curves whereas the red dots indicate observed dispersion)	62

Figure A.8: S-wave velocity profile at Wien 2 (Radius: 10m)	63
Figure A.9: SPAC spectrum at Wien 2 for radius 20m	63
Figure A.10: Dispersion curve at Wien 2 for radius 20m (Black curves indicate theoretical dispersion curves whereas the red dots indicate observed dispersion)	64
Figure A.11: S-wave velocity profile at Wien 2 for radius 20m	64
Figure A.12: SPAC spectrum at Wien 2 for radius 40m	65
Figure A.13: Dispersion curve at Wien 2 for radius 40m	65
Figure A.14: S-wave velocity profile at Wien 2 for radius 40m	65
Figure A.15: SPAC spectrum at Wien 2 for radius 80m	66
Figure A.16: Dispersion curve at Wien 2 for radius 80m (Black curves indicate theoretical dispersion curves whereas the red dots indicate observed dispersion)	67
Figure A.17: S-wave velocity profile at Wien 2 for radius 80m	67
Figure A.18: SPAC spectrum at Wien 2 for radius 160m	68
Figure A.19: Dispersion curve at Wien 2 for radius 160m (Black curves indicate theoretical dispersion curves whereas the red dots indicate observed dispersion)	68
Figure A.20: S-wave velocity profile at Wien 2 for radius 160m	68
Figure A.21: SPAC spectrum at Wien 2 for multiple solutions	69
Figure A.22: Dispersion curve at Wien 2 for multiple solutions (Black curves indicate theoretical dispersion curves whereas the red dots indicate observed dispersion)	69
Figure A.23: S-wave velocity profile at Wien 2 for multiple solutions	70
Figure A.24: S-wave velocity profile at Wien 2 for multiple solution	71

CHAPTER 1

INTRODUCTION

1.1 General

Earthquakes are major natural disasters that cause severe social, economic and structural losses. It is not yet possible to forecast the earthquakes but it is possible to reduce the losses resulting from these catastrophes. Thus, for purposes of disaster mitigation, interdisciplinary studies related to earthquakes have become popular among researchers including geological, geophysical and civil engineers.

Nowadays, it is well-known that structural damage caused by the earthquakes depends not only on the magnitude and wave propagation properties but also on the soil properties. Soft soil layers on top of hard bedrock can greatly amplify the ground motions yielding severe structural damage. This is in particular the case when the resonance frequency of the soil and building are close to each other. As a result, site characterization is critical in terms of disaster mitigation.

For the estimation of dynamic properties of soils (including the fundamental frequencies and amplification factors), traditional methods such as seismic refraction, reflection and drilling are used commonly in geotechnical and geophysical engineering fields. However, with these difficult and costly methods, it is not always feasible and possible to obtain the S-wave velocity of the deep soil layers. In addition, in urban areas invasive methods are not easy to apply. Thus, as an alternative to the existing methods in the literature for measuring S-wave velocities, surface wave techniques are used commonly. Surface wave techniques are categorized with respect to their source properties: active sources and passive sources. When an artificial source is used to create waves within the soil, the technique is called active seismic method. On the other hand, surface wave methods, which employ ambient vibrations of the earth (microtremors), are called passive seismic methods. Both active and passive techniques are based on the same principle: the theoretical dispersion curve of a model velocity profile is matched with the measured dispersion curve by a series of iterations. While active methods are not suitable for deeper layers and are very expensive, passive seismic techniques are less expensive and are much more efficient to resolve the deeper part of the soil. Nowadays for practical purposes, V_{s30} (Average shear wave velocity in top 30m of soil layers) is used as the direct and only measure for site classification. However, numerical experiments clearly indicate that the depth of bedrock and resolution of soil layers affect the fundamental frequency and corresponding amplification factors significantly. Thus, it is essential to resolve the deeper soil layers for accurate estimates of the dynamics properties at a site of interest.

Among existing alternative methods for evaluating passive sources, the most efficient method for the interpretation of microtremor data is the Multi-Mode Spatial Autocorrelation (MMSPAC) technique. This method detects for the higher modes of seismic energy as well as the fundamental mode to estimate the S-wave velocities independent of the direction. In addition, this method works efficiently even with a small number of stations. As of today, all

over the world there are many MMSPAC applications. However, number of such studies is very limited for Turkey. The heterogeneous basins located on the North Anatolian Fault zone are indeed ideal places for such applications to estimate the sedimentary thicknesses and bedrock levels.

In the long run, results of this study and similar studies could be used to construct two-or three-dimensional regional velocity models. Examples of such models exist for many seismic regions in world. These models can be used for several applications in various fields ranging from wave propagation simulations to seismic hazard assessment.

1.2 Objectives and Scope

This study presents a case study for site characterization with alternative geophysical and geotechnical techniques in sedimentary basins on the North Anatolian Fault zone in Turkey. There are two main objectives of this thesis: First, one is to apply alternative methods to compute the fundamental frequencies and amplification factors of soft soils located in seismically active urban regions. Second objective is to compare the results with each other and assess the comparative effectiveness of each method.

The structure of the thesis is as follows:

In Chapter 2, applications of the Multi-Mode Spatial Autocorrelation Method for Düzce and Bolu case studies are presented. Microtremor data are collected and interpreted at selected sites in Düzce and Bolu city centers. The collected data are used to form coherency curves. From the (pseudo) inverse solutions of these curves, the variation of S-wave velocities with respect to depth is obtained. The results obtained from the MMSPAC technique in this chapter will be used as input to site response analysis for estimating the amplification factors in Chapter 3.

In Chapter 3, two alternative methods for site amplifications are applied. The first technique includes Horizontal to Vertical Spectral Ratio (HVSr) analyses of both microtremor and strong ground motion data collected at Bolu and Düzce stations. The second technique is One-dimensional Site Response Analysis using theoretical transfer functions. In this method, analyses are performed with the S-wave velocity profiles obtained from the microtremor analyses in Chapter 2. The results are presented in the form of one-dimensional velocity structure and comparisons of frequency-dependent site amplifications from alternative techniques at the selected sites.

In Chapter 4, main findings of this thesis are summarized along with the conclusions derived from the analyses. In addition, recommendations for future studies are presented.

The related literature is discussed in detail within each Chapter.

CHAPTER 2

ESTIMATION OF ONE-DIMENSIONAL SHEAR WAVE VELOCITY PROFILES WITH MULTI-MODE SPATIAL AUTOCORRELATION METHOD (MMSPAC)

2.1 General

Nowadays, traditional methods like seismic refraction, reflection and drilling are used commonly for estimation of dynamic properties of soils. However, with these difficult and costly methods, it is not possible to obtain the S-wave velocity of the deep soil layers. As an alternative to the existing methods in the literature for measuring S-wave velocities, surface wave techniques are used commonly. Surface wave techniques are categorized with respect to their source properties: active sources and passive sources. Hammers, weight drops, electromechanical shakers, seismic vibrators and bulldozers are instruments used as active sources.

In the literature, there are two popular methods which mainly use active sources: Spectral Analysis of Surface Waves (SASW) (Nazarian and Desai, 1993; Kramer, 1996; Zywicki, 1999) and Multi-Channel Array Surface Waves (MASW) (Park et al., 1999) techniques. These techniques are based on the same principle: the theoretical dispersion curve of a model velocity profile is matched with the measured dispersion curve by a series of iterations (Rosenblad and Li, 2009).

On the other hand, surface wave methods which employ ambient vibrations of the earth (microtremors) are called passive seismic methods. Passive Refraction Microtremor (ReMi) (Louie, 2001), Frequency-Wavenumber (f-k) (Schmidt, 1986), Spatially Autocorrelation (SPAC) (Aki, 1957) and Multi-Mode Spatial Autocorrelation (Asten et al., 2003) are the most common passive seismic methods.

Among these alternative methods, the most efficient method for the interpretation of microtremor data is the MMSPAC technique. This method resolves for the higher modes of seismic energy as well as the fundamental mode and estimates the S-wave velocities independent of the direction.

2.2 Microtremors (Microseism)

The continuous low-amplitude vibrations within the Earth which are not a result of any seismic activity are called microtremors (microseism). These vibrations are generated by the human activities (such as machinery, cars and people walking) with the frequency bands higher than 1 Hz and natural events (such as rain, wind, atmospheric pressure differences and ocean waves) with the frequency bands less than 1 Hz. Following are the main properties of microtremors (Asten, 1976):

- The energy generated by oceans or coastlines is in a period range of 10 to 1 sec. It can be propagated for hundreds or thousands of kilometers.

- The energy generated by atmospheric loading effects is in a period range of 100 to 1 sec.
- The energy generated by wind action is in a period range of 100-1 sec. It cannot be propagated for distances greater than 1 km.
- The energy generated by human activities such as machines and traffic is in a period range of 0.03 to 1 sec.

Due to the aforementioned sources (human activity and natural events), microtremors have differences with time and are not repeatable. Because the amplitude content of the microtremors is between 10^{-4} to 10^{-2} mm, the microtremors cannot be perceived by the human (Okada, 2003; Roberts and Asten, 2004). In the microtremor phenomenon, records are both comprised of body and surface waves although most of the passive wave energy is transported as surface waves (Toksöz and Lacoss, 1968; Roberts and Asten, 2004).

2.3 The Microtremor Survey Method (MSM)

The Microtremor Survey Method is a practical field method for determining the properties of the dispersion of the surface waves. To perform this method, the soil at the selected site should consist of homogenous, isotropic and parallel geological layers.

The basic steps of the microtremor survey method are the following (Okada, 2003):

- Recording of the natural noise with a seismometer at a selected site.
- Determining response of the subsurface layers below the array with the dispersion of the surface waves.
- Inversion of the dispersion curve with an appropriate algorithm for determining the shear wave velocity profile.

Among the microtremor survey methods, SPAC method is an efficient tool to detect the surface waves in records of the microtremor. Following are the main properties of SPAC method (Aki, 1957; Okada, 2003):

- Microtremors are assumed to be stochastic processes in time and space.
- A spatial autocorrelation coefficient can be determined when the waves forming the microtremors have dispersive behavior like surface waves.
- The spatial autocorrelation coefficient is a function of frequency and phase velocity.

2.4 Implementation of SPAC Method

Implementation of the traditional SPAC method for extracting S-wave velocity profile is demonstrated in Figure 2.1. In this classical approach, the following main steps are performed:

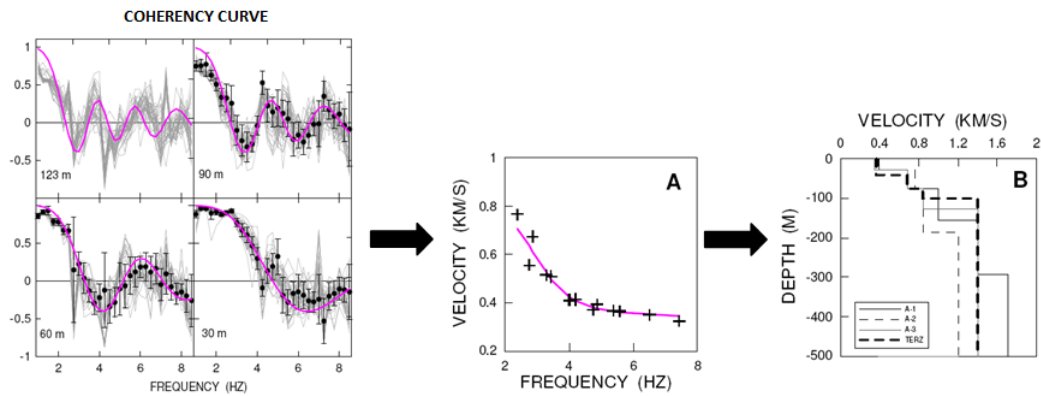


Figure 2.1: Main steps of traditional SPAC Implementations (Figure is adapted from Maresca et al., 2006)

- a) Collection of the SPAC data acquisition
- b) Computing the SPAC spectrum from array measurements
- c) Determination of the observed surface wave dispersion curve. The dispersion curve is plotted as phase velocity, $v(f)$, versus frequency, f .
- d) Inversion of the dispersion curve for an S-wave velocity profile with one of the suitable algorithms for surface-wave inversion (Asten, 2006a).

2.4.1 Collection of SPAC Data and Properties of Array Geometry

In SPAC method, data is collected using three-component seismometers. Use of seismometers with three-components helps for detection of both Love and Rayleigh waves.

In the classical SPAC method, data is collected as follows: The microtremors are recorded with seismometers connected to each other (Figure 2.2) where all seismometers are synchronized with GPS equipment (Okada, 2003).

Okada (2003) demonstrated that microtremors recorded at night are more convenient than daytime in terms of minimizing the noise created by human activities. Although the duration of the record is mostly 45 min. or 60 min. for long period microtremors, generally 30 min records are enough for short period microtremors.

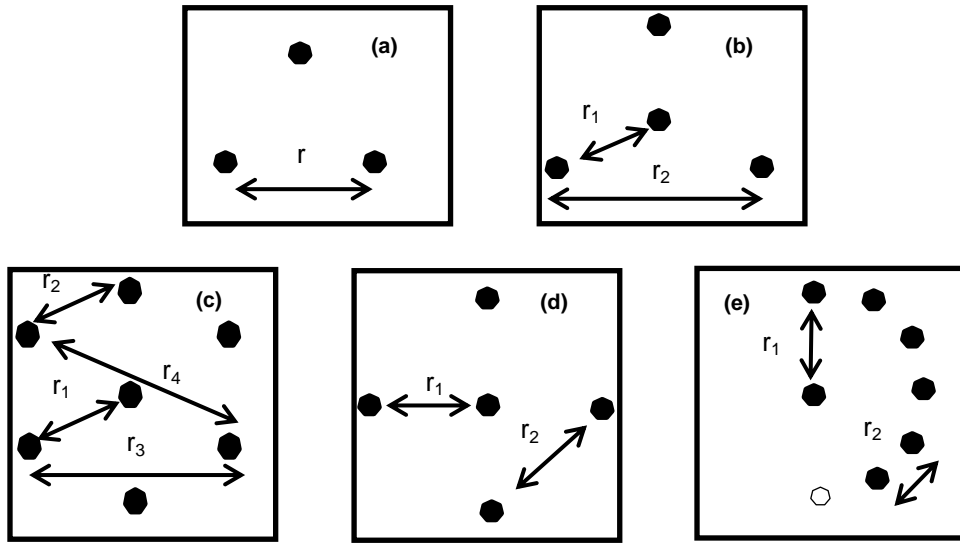


Figure 2.2: Array geometries for SPAC method used in literature. (a) and (b) demonstrate triangular arrays (c) is a hexagonal array, (d) is a square or a linear cross array, and (e) is a semi-circular array (Figure is adapted from Asten, 2004).

2.4.2 Calculation of the SPAC Coefficient

In the original study by Aki (1957), the traditional SPAC method was introduced to derive S-wave velocity structure based on the coherency of microtremor records. The method is built on the theoretical framework of a stochastic wavefield which is stationary in both time and space. The traditional SPAC method uses the vertical wavefield acquired by seismometers in a circular or semicircular array (Figure 2.3). Aki (1957) showed that:

$$\bar{\rho}(f, r) = J_0(2\pi fr/v(f)) \quad (2.1)$$

where $\bar{\rho}(f, r) = \int_0^{2\pi} \rho(r, f, \theta) d\theta$ is the spatially (and azimuthally) averaged coherency for interstation distance r and frequency f . In Equation 2.1, J_0 indicates the Bessel function of the first kind and zero order that identified Rayleigh phase velocity $v(f)$ for a given f , or relation of the dispersion.

Measured coherency is identified as the following normalized cross-power spectra:

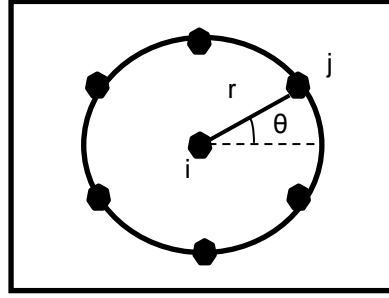


Figure 2.3: Circular layout for microtremor measurement with traditional SPAC method

$$C_{ij}(f) = \frac{(S_i(f) \cdot S_j^*(f))}{\left((S_i(f) \cdot S_i^*(f)) \cdot (S_j(f) \cdot S_j^*(f)) \right)^{1/2}} \quad (2.2)$$

where $C_{ij}(f)$ is the complex spectral coherency, $S_i(f)$ and $S_j(f)$ are complex Fourier spectra at stations i and j . In addition “*” indicates complex conjugate of S . This way the cross power spectra can be calculated for each seismometer pair of the array at a given interstation distance r (Stephenson and Odum, 2011). The difference between modeled and observed SPAC curves must be minimum for the “correct” S-wave velocity structure at a site of interest.

2.4.3 Estimation of the Phase Velocity with Traditional SPAC Method for Near-Surface Structure

In a standard record of Rayleigh waves, first mode is more dominant than the higher modes. In addition, the theoretical Rayleigh wave motion assumes that the geological layers of the surface consist of horizontal layers. Phase velocity is calculated for determining the S-wave velocity profile using the microtremor recordings. For performing this procedure, inversion is used on microtremors. Traditional SPAC inversion includes the following steps:

1. Computing the differences between measured and calculated phase velocities for each frequency bin.
2. Soil parameters are selected to identify the subsurface velocity profiles.
3. Iterations are performed on selected parameters until the misfit is minimized.

This procedure is applied until the measured and calculated spectra match each other.

For determining the phase velocity of the Rayleigh waves as a function of frequency for a circular or semicircular array (with radius r) measurement, $A = 2\pi r_0 (r = r_0)$ is accepted as a constant.

Equation for SPAC coefficient (2.1) can be written as:

$$\rho(f, r) = J_0\left(\frac{Af}{v}\right) = J_0(x) \quad (2.3)$$

Where $x = \left(\frac{Af}{v}\right)$ and J_0 is first kind and zero order Bessel function. The simplicity of Equation (2.3) appears to suggest a possibility of easily finding the optimum Bessel function $J_0(x)$ from a range of observed values of " $\rho_{r_0}(f)$ " by the least-squares fitting model. However, the solution to the Equation (2.3) is theoretically not unique.

In practice,

$$v(f) = Af/x \quad (2.4)$$

Provides a solution for the phase velocity where:

$$x_0 = 2\pi f_0 r_0 / v(f_0) \quad (2.5)$$

And phase velocity for frequency f_0

$$v(f_0) = \frac{2\pi f_0 r_0}{x_0} \quad (2.6)$$

2.5 Implementation of MMSPAC Method

Okada (2003) and several other authors who used the SPAC method have calculated the coherency spectrum and then inverted the phase velocity dispersion curve. These authors, basically fit the modeled and observed phase velocity dispersion curves to evaluate the S-wave velocity profile at a site of interest.

An alternative approach to the SPAC method is introduced by Asten et al. (2002; 2004) and Wathelet et al. (2005). The goal of this alternative approach is to fit the observed SPAC spectra directly to modeled SPAC spectra (Asten, 2006a). In other words, dispersion curve is not directly inverted but rather checked simultaneously while fitting the observed and SPAC modeled curves.

A fundamental advantage of the MMSPAC method is identification of the higher mode surface wave energy (Asten, 2004), and mitigation of Vs bias by calculating of azimuthal averaging (Stephenson and Odum, 2011). Application of this method can be summarized in two major steps:

- a) Collection of the data in the field
- b) Data analyses within a computational framework

These steps will be briefly discussed in the following subsections.

2.5.1 Collection of MMSPAC Data and Properties of Array Geometry

Standard procedure for the MMSPAC data collection is demonstrated in Figure 2.4. It starts with the selection of the field. The study field should be located in a silent area to omit undesirable noise. After the set up and synchronization all of seismometers, recording is started. All seismometer records in pairs are used for calculation of the Vs velocity model. However, in rare examples, one of the four seismometers' records can be omitted from interpretations due to the poor intra-array coherency (Stephenson and Odum, 2011).

2.5.2 Pre- processing and Data Analyses in MMSPAC Method

Data processing starts with an initial velocity profile that consists of P-wave velocity (V_p), S-wave velocity (V_s), ρ (density), and depth values (Figure 2.5(a)). The initial model is generally selected from previous information on the lithology of the site of interest. Figure 2.5 (b) demonstrates the observed and modeled SPAC spectrum. The modeled SPAC spectrum is calculated by first computing the theoretical phase velocity dispersion curve with open-source codes of Herrmann (2001). (Figure 2.5(d)). The algorithm of Herrmann (2001) uses matrix methods introduced from Saito (1979, 1988).

Figure 2.6 describes the major stages of the computational framework used for interpretation of MMSPAC field data. In step 1 the related data with respect to recording date and time is selected. A single time window is used for each interpretation. The selected time window is extracted from the record to get rid of large amplitude spikes and noise in the records. In addition, Hann window filtering is used for each selected time series. Then, Fast-Fourier Transformation is performed for computing SPAC coherency spectrum of Equation 2.2. In the step 2, the selection of the different format types such as USGS Sud format, Guralp Sac format or others is performed. Then, average coherency curves are plotted. In step 3, single or multiple SPAC files first is selected. Then, forward fitting is started with an initial velocity profile until observed and modeled SPAC coherency curves match each other. The goodness of the fit between the observed and modeled SPAC coherency is measured by the Root Mean Square (RMS) error over a frequency range of interest. At the end of the interpretation, the results are presented in the form of V_s versus depth profiles.

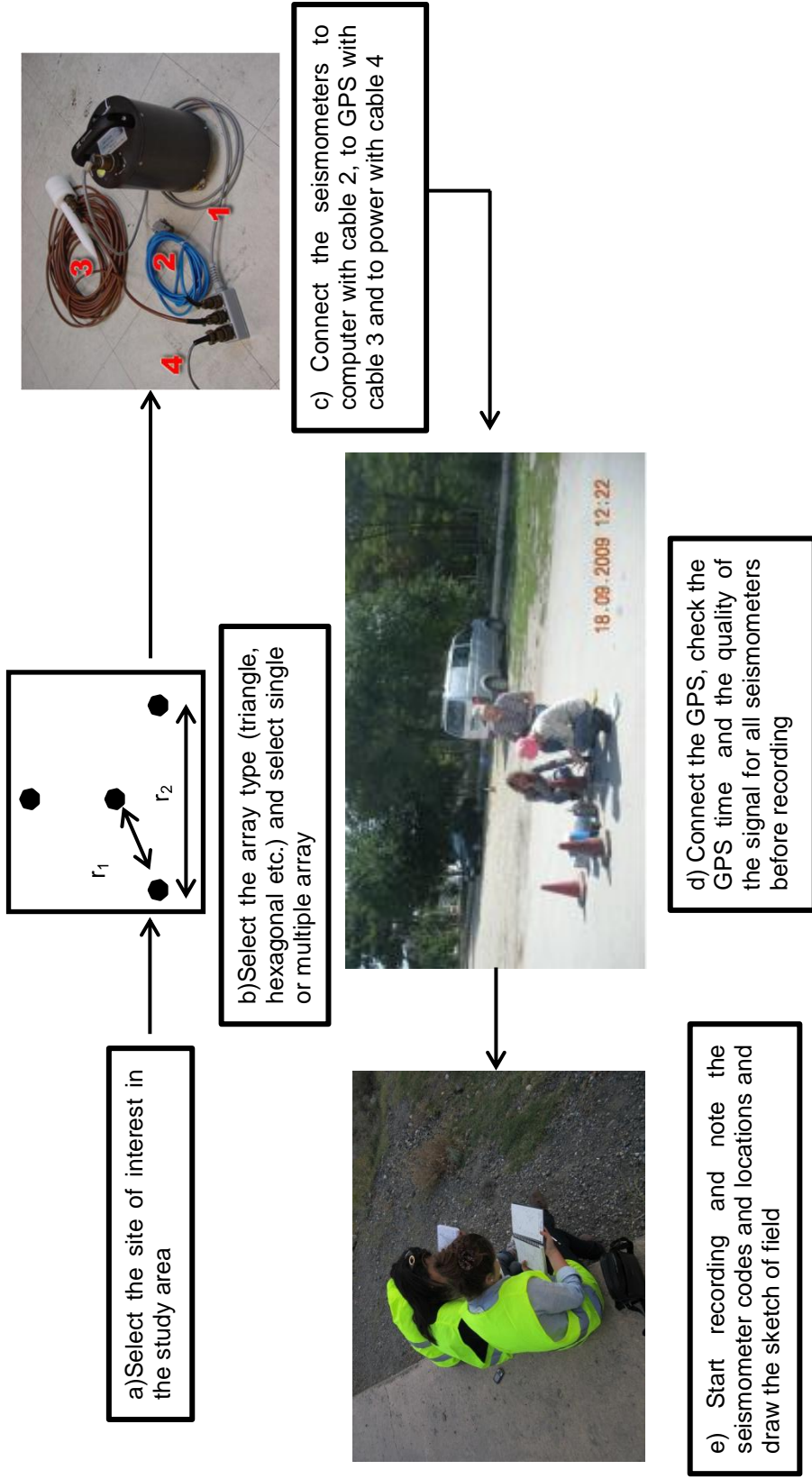


Figure 2.4: Step by step description of a typical MMSPAC field work

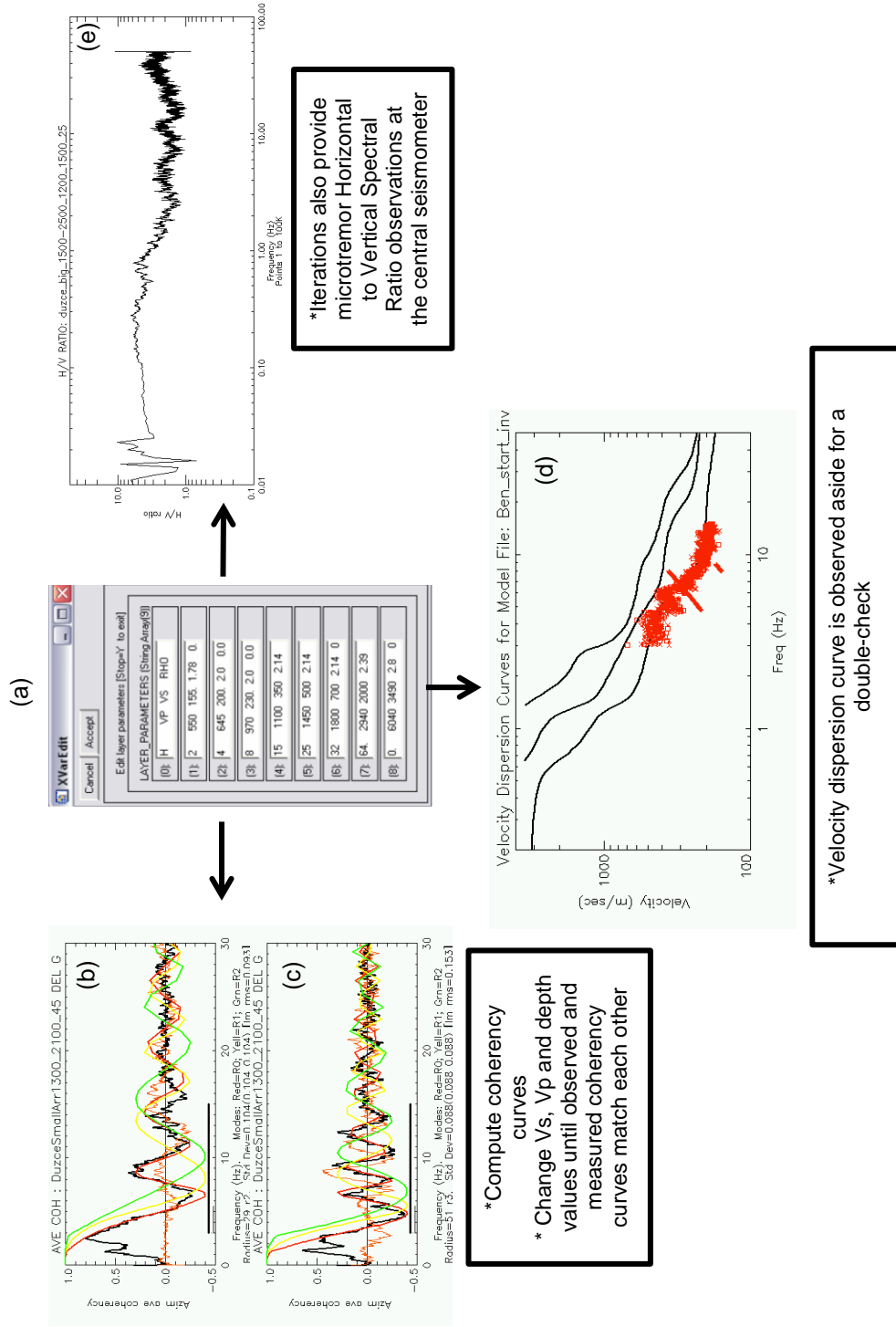


Figure 2.5: Major steps of MMSPEC implementation

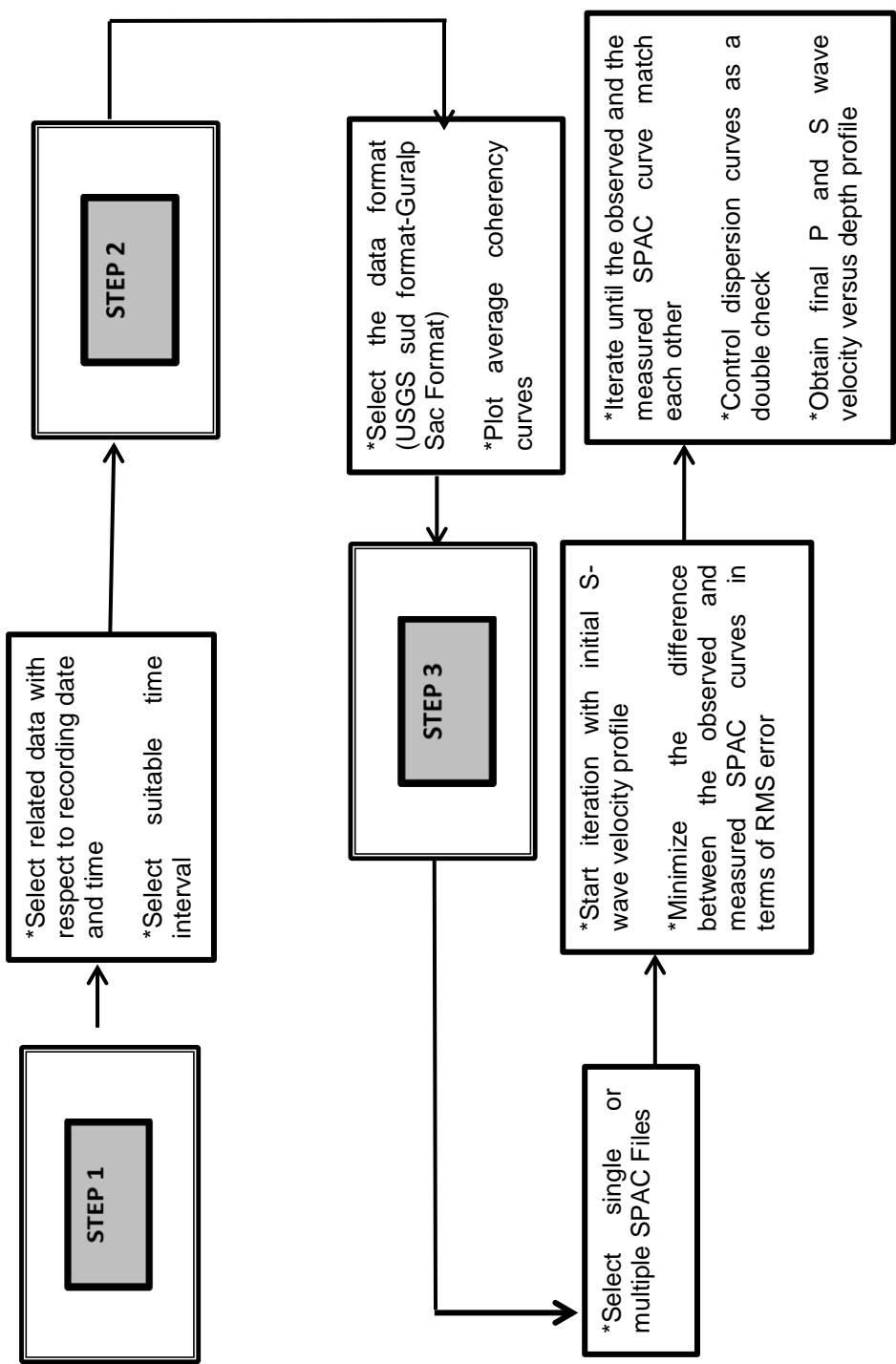


Figure 2.6: Flowchart for the computer implementation of MMSPAC method

2.6 Study Areas: Düzce and Bolu

This section of the thesis presents a series of attempts to perform site characterization with microtremor survey technique at two strong motion stations (DZC and BOL sites) in Düzce and Bolu.

The geology of North-Western Anatolia ranges from hard Mesozoic bedrock in mountain ranges to large sediment-filled, pull-apart basins. Düzce and Bolu city centers are located in major alluvial basins in the region, both of which have suffered from severe building damage during the 12 November 1999 Düzce earthquake ($M_w=7.1$). Düzce and Bolu basins are tensional basins, which have formed within the dextral shear system of the North Anatolian fault (Figure 2.7). The two basins include coarse fluvial sediments of Miocene age and younger, overlain by lacustrine sediments of Pleistocene age. The thickness of Miocene and later sediments is given by Şengör et al. (2005) as approximately 260m for Düzce, and up to 200m for Bolu. The basement is mainly volcanic flysch of Eocene age. Figure 2.8 presents the geological maps of Düzce and Bolu. In addition, stars indicate the location of the strong ground motion stations where the measurements are taken. The MMSPAC method is applied adjacent to buildings containing strong-motion accelerometers installed at Düzce and Bolu as part of the Turkish National Strong Ground Motion Network.

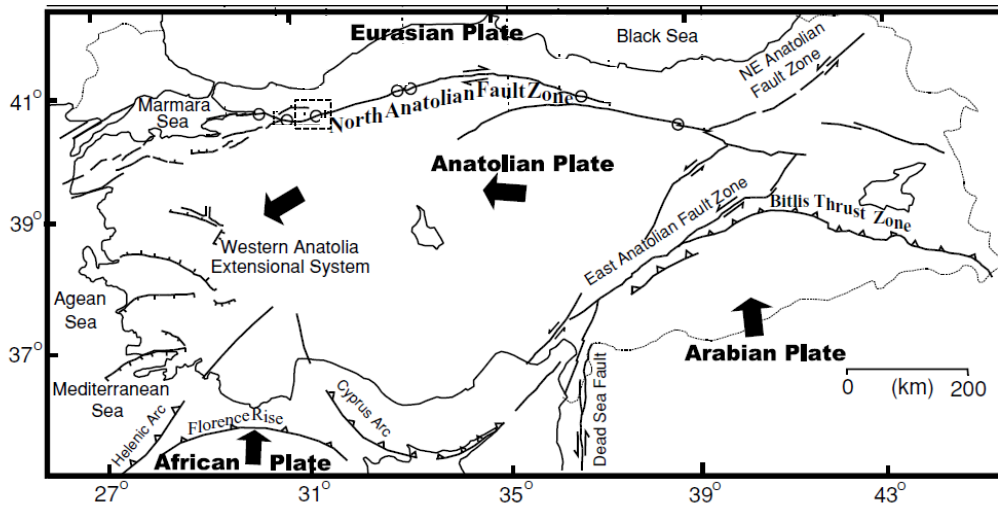


Figure 2.7: Map demonstrates tectonic settings of Turkey. The dashed rectangle indicates the study areas and large arrows represent the direction of relative plate motions. (Figure is adapted from Utku et al., 2003).

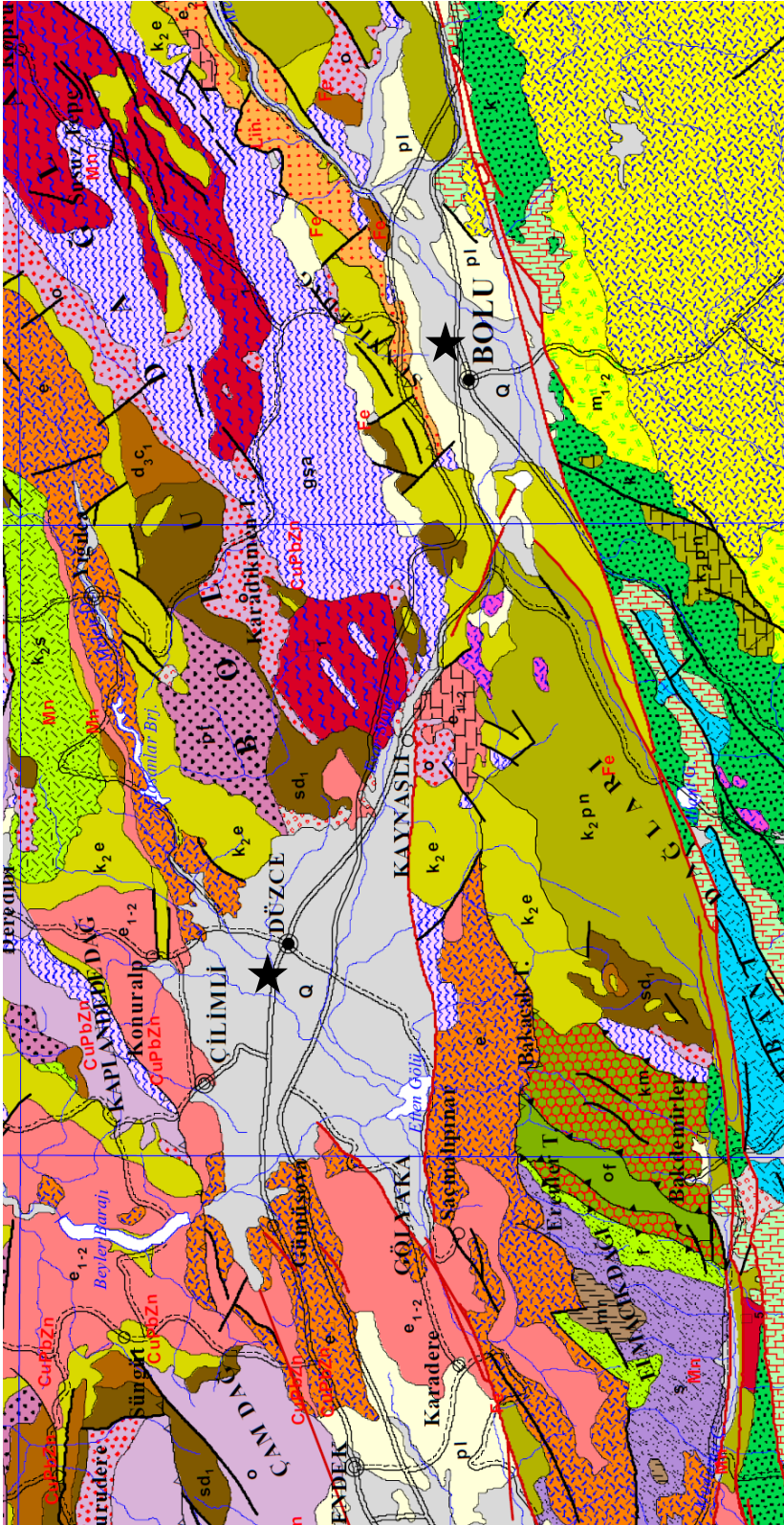


Figure 2.8: Geological map of Düzce and Bolu (Grey areas are undifferentiated Quaternary at Düzce and Bolu. Stars indicate the location of the strong ground motion stations where the measurements are taken.) (Figure is adapted from www.mta.gov.tr)

2.6.1 Previous Microtremor and Surface-Wave Surveys in the Region

In this section, a summary of previous studies for determining S-wave velocity profiles using geophysical and geotechnical methodologies like drilling, seismic refraction, Re-Mi, SPAC, SASW, Borehole and Standard Penetration Test (SPT) in Düzce and Bolu are presented. Summary of information on velocities and depths obtained in these studies are demonstrated in Table 2.1. In addition, S-wave velocity profiles are shown in Figures 2.9-2.19. It must be noted that all of these studies are performed at the same location i.e. strong ground motion stations.

Table 2.1: Information on the previous studies for determining S-wave velocity profiles in Düzce and Bolu

Study	Method	Study Area	Maximum Depth Resolved (m)
Kudo et al. (2002)	SPAC	Düzce	~500
Yamanaka et al. (2002)	f-k	Düzce	~1000
Rosenblad et al. (2006)	SASW	Düzce	50
Yılmaz et al. (2008a, 2008b)	SASW, Borehole, MASW	Düzce	50
Alexoudi (2008)	SPAC	Düzce	~250
Tokgöz (2002)	Refraction	Bolu	30
Başokur (2005)	Re-Mi	Bolu	64
Rosenblad et al. (2006)	SASW	Bolu	50
Ansal et al. (2007)	SPT	Bolu	~100

From Figures 2.9-2.19, it is observed that the passive techniques are generally able to resolve the velocity structure down to deeper layers. This is expected, as the active sources do not penetrate into the deeper parts of the soils. On the other hand, it is also observed that even the same technique used by different authors can yield not exactly the same profiles. This indicates the non-uniqueness of the mathematical inversions. That is also why in this thesis; a pseudo-inverse approach is taken via an iterative forward fitting algorithm. This way, it is possible to get a more physical solution rather than getting stuck at any local minimum that the inversion algorithms usually converge to. Next, the field work for MMSPAC technique is described.

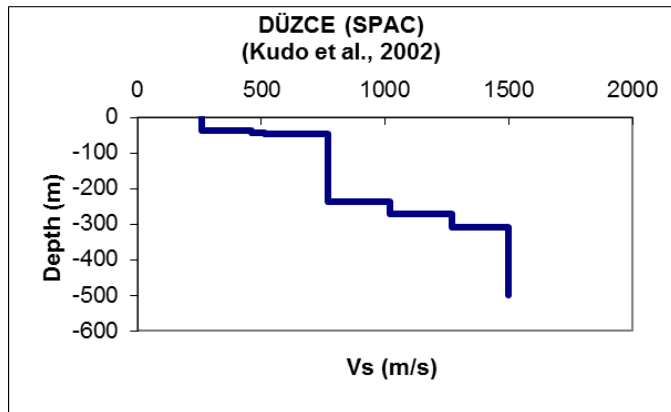


Figure 2.9: Düzce site: S-wave profile obtained by Kudo (2002)

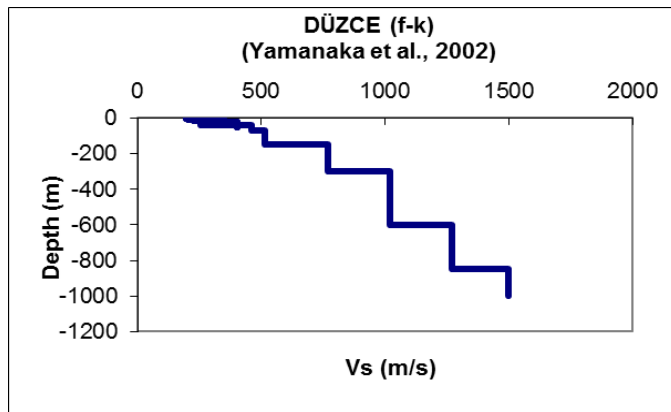


Figure 2.10: Düzce site: S-wave profile obtained by Yamanaka (2002)

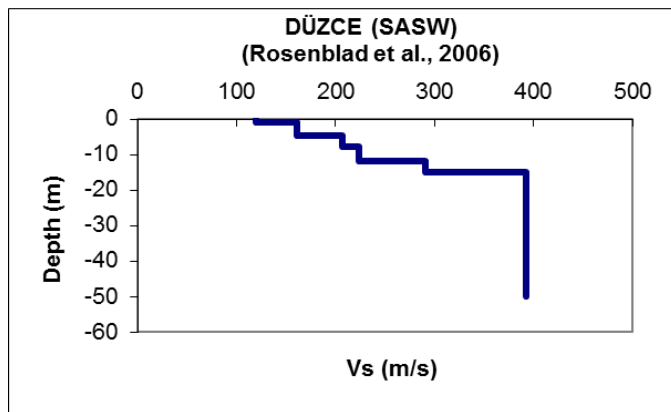


Figure 2.11: Düzce site: S-wave profile obtained by Rosenblad (2006)

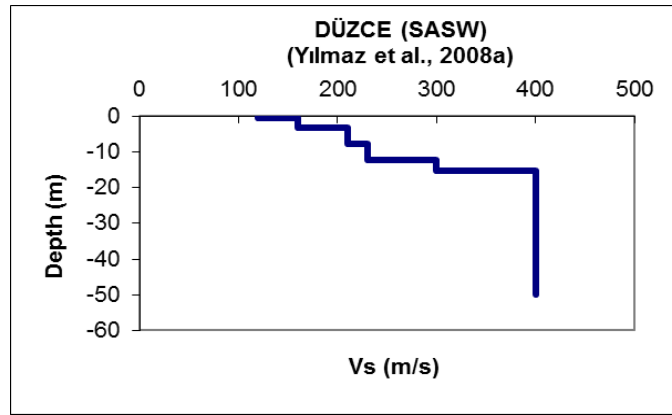


Figure 2.12: Düzce site: S-wave profile obtained by Yılmaz et al. (2008a)

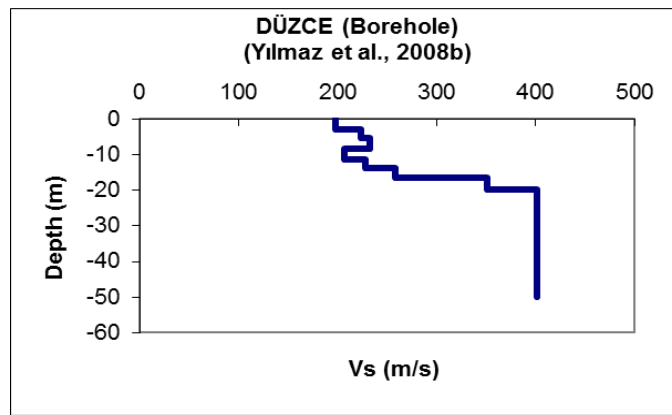


Figure 2.13: Düzce site: S-wave profile obtained by Yılmaz et al. (2008b)

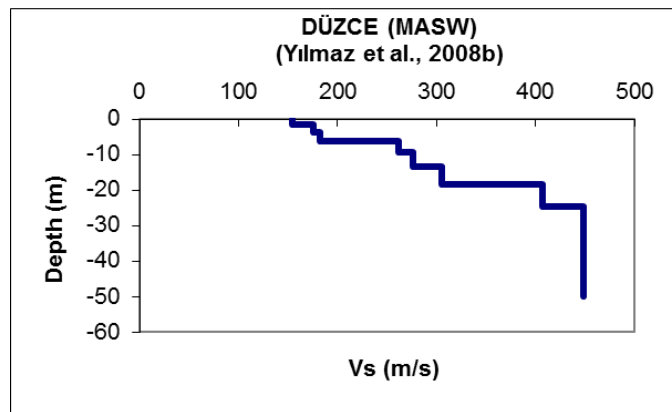


Figure 2.14: Düzce site: S-wave profile obtained by Yılmaz et al. (2008b)

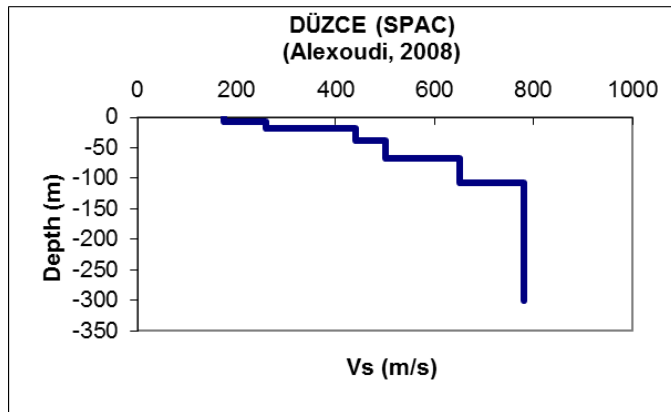


Figure 2.15: Düzce site: S-wave profile obtained by Alexoudi (2008)

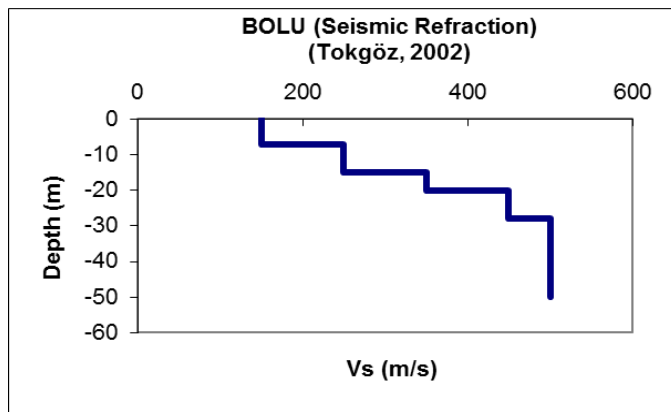


Figure 2.16: Bolu site: S-wave profile obtained by Tokgöz (2002)

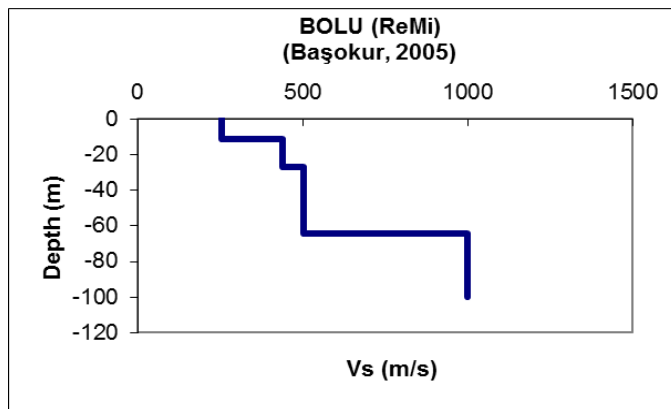


Figure 2.17: Bolu site: S-wave profile obtained by Başokur (2005)

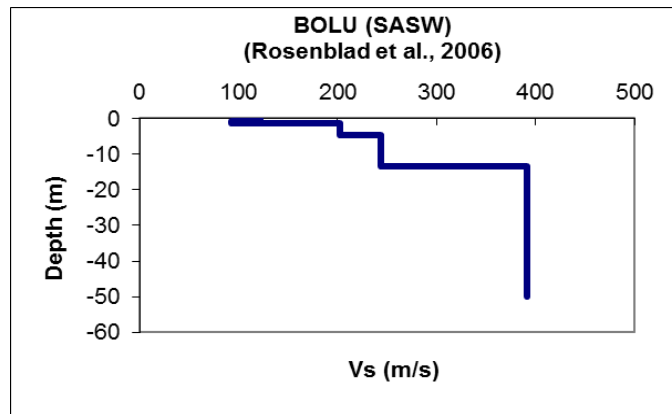


Figure 2.18: Bolu site: S-wave profile obtained by Rosenblad et al. (2006)

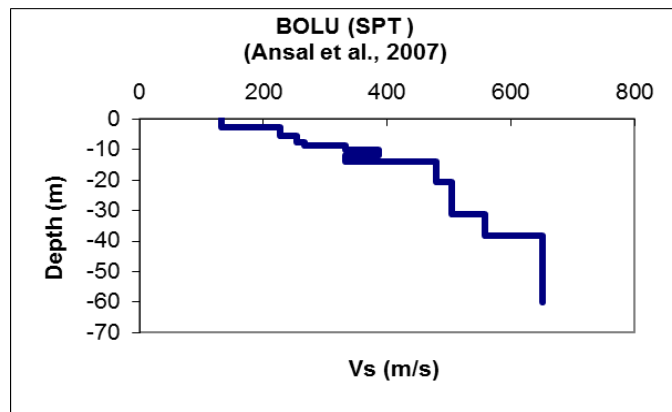


Figure 2.19: Bolu site: S-wave profile obtained by Ansal et al. (2007)

2.6.2 MMSPAC Array Data in Düzce and Bolu

Recording instruments are three components Guralp CMG6TD seismometers containing internal data recorders, GPS sensors and a crystal clock synchronizable with a GPS signal (Figure 2.20 (a)). The seismometer is sensitive to ground vibrations over a frequency range 0.033-50 Hz as standard. Array geometry performed in Düzce and Bolu sites is demonstrated in Figure 2.20 (b) along with the sketch maps in Figures 2.20 (c) and Figure 2.20 (d), respectively. At Düzce, two nested four-station triangular arrays with side-lengths 30m and 90m are used, with a common baseline on the same road. At Bolu, a single triangular array of side-length 33.3m is placed on an asphalt-surfaced car-park.

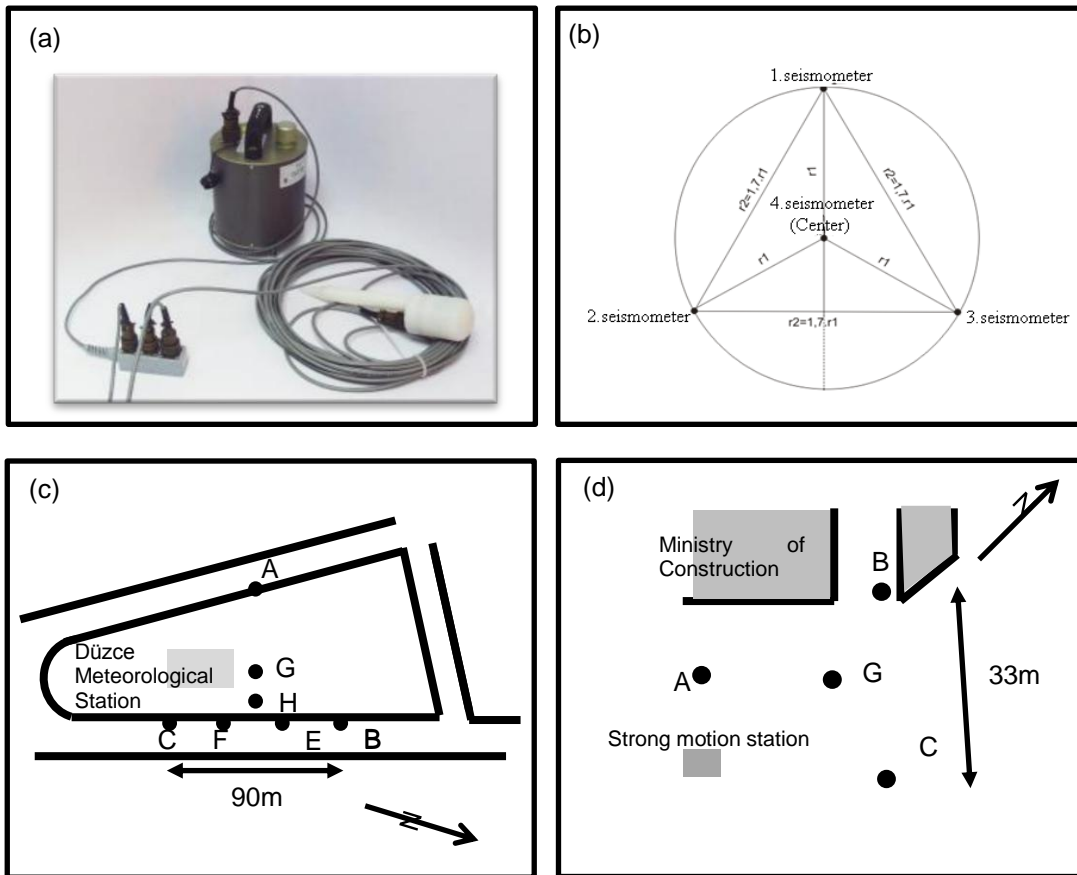


Figure 2.20: a) Guralp CMG6TD seismometer (Figure is adapted from <http://www.guralp.com>) b) Standard centered-triangular arrays c) Sketch map of arrays at Düzce Strong Ground Motion Station d) Sketch map of array at Bolu Strong Ground Motion Station

Each seismometer is placed on the asphalt surface and covered with a plastic bucket to provide some degree of shielding from wind and sun. For data processing, Asten (2006a) is followed using data segments with typical durations of 20 minutes selected from total recording times of about 40 minutes. Vertical-component data is used although it is noted that a modified methodology making use of three components in the MMSPAC method have been used in other studies (e.g.: Cho et al., 2006; Köhler et al., 2007; Garcia-Jerez et al., 2008). In this application, there is an important assumption that the propagating seismic noise consists of dominantly fundamental-mode Rayleigh waves, where sources are sufficiently distant to produce plane waves across the array. The sampling rate is 100 Hz.

2.6.3 Results from MMSPAC Interpretations for Düzce and Bolu

From the selected data based on the previously-explained algorithms, SPAC dispersion curves are obtained. In Figures 2.21, 2.23 and 2.26 black curve indicates real part of MMSPAC field data whereas thin red curve is an imaginary part of the SPAC field data. In addition, modeled SPAC curves for modes fundamental, first and second (R0, R1, R2) are

shown with thick red, yellow and green curves in the figures, respectively. In Figures 2.22, 2.24 and 2.27 dispersion curves are displayed for the first and higher modes.

These implementations are termed the multimode SPAC method because while the fitting is performed using the modeled fundamental Rayleigh mode (R0), the simultaneous plotting of modeled SPAC spectra for the first and second higher modes (R1, R2) allows identification of frequency bands where higher-mode energy is present. The presence of higher-mode energy is best seen when the same time segment of data is recorded for two or more station separations. Thus in Figure 2.21 and 2.23 the observed SPAC in the frequency band 4-5 Hz shows a clear shift towards the R_1 model curve indicating presence of mixed-mode energy propagation.

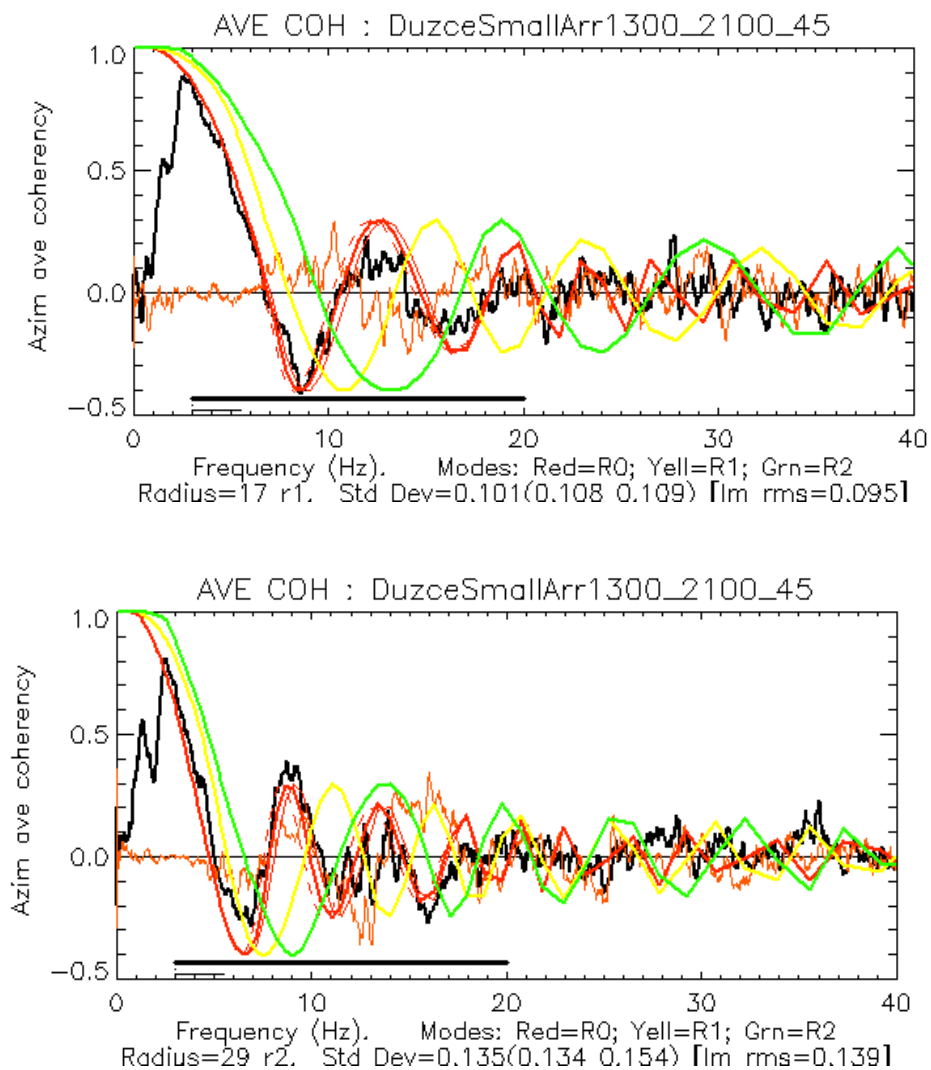


Figure 2.21: SPAC spectra at Düzce (small array) (Top Panel: SPAC spectra for r1, Bottom Panel: SPAC spectra for r2)

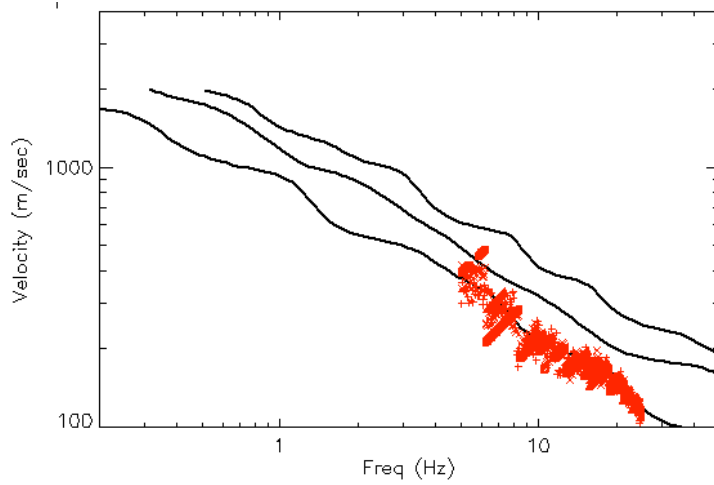


Figure 2.22: Dispersion curve at Düzce (small array) (Black curves indicate theoretical dispersion curves whereas the red dots indicate observed dispersion)

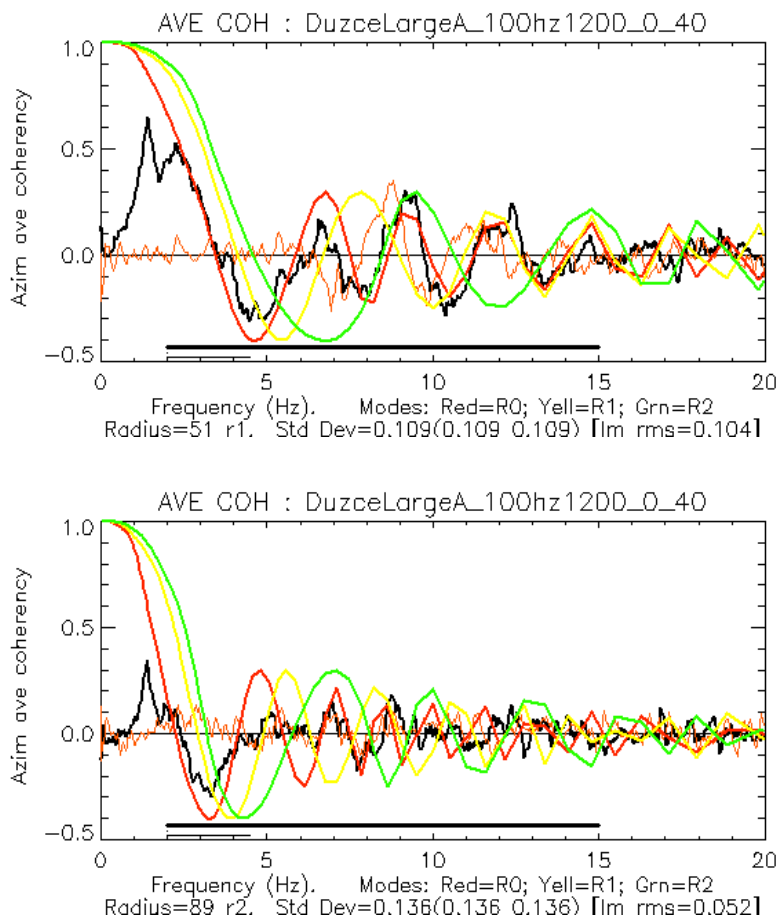


Figure 2.23: SPAC spectra at Düzce (large array) (Top Panel: SPAC spectra for r1, Bottom Panel: SPAC spectra for r2)

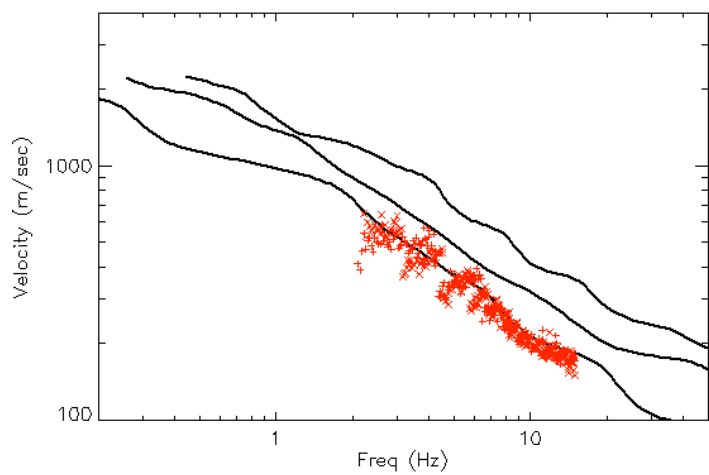


Figure 2.24: Dispersion curve at Düzce (large array) (Black curves indicate theoretical dispersion curves whereas the red dots indicate observed dispersion)

In addition, the useful low-frequency limit of the SPAC data at both sites is approximately 2 Hz, despite the fact that the seismometers used had a flat pass band from 0.016 Hz to 50 Hz. This is a common problem where Guralp seismometers are set up on pavements (see Roberts and Asten, 2007 and Claprod et al., 2011). When the seismometers are buried, useful SPAC data is typically obtained down to frequencies of order 0.1 Hz (see Asten, 2005; Stephenson et al., 2009 and Schramm et al., 2012). The useful high-frequency limit is highly dependent on local conditions and the lateral uniformity of the layered earth. The high frequency limit at Düzce is 25 Hz. The S-wave velocity profile for Düzce obtained after a series of iterations is given in Figure 2.25 and Table 2.2.

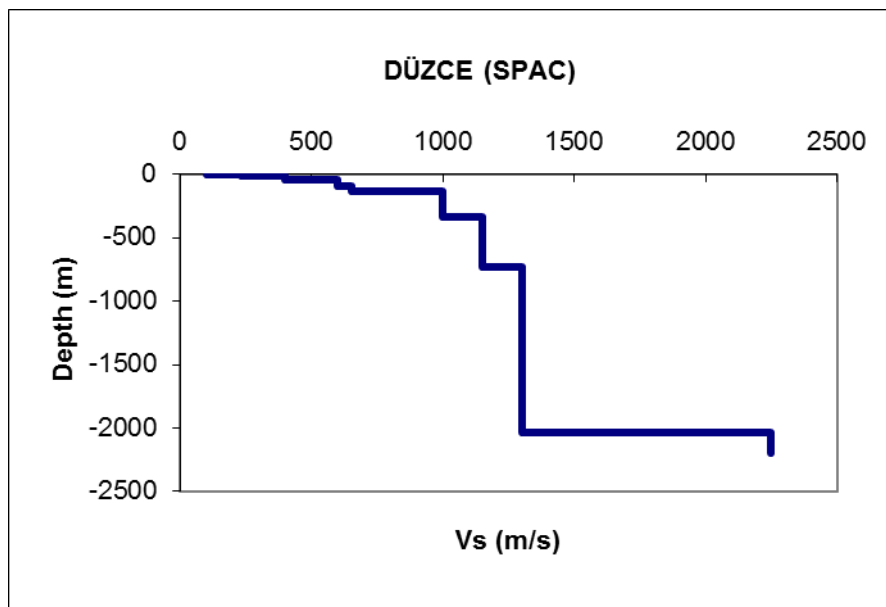


Figure 2.25: S-wave velocity profile at Düzce

The SPAC spectra for Bolu are shown in Figure 2.26. The high frequency limit at Bolu is 20 Hz (at Bolu, the center station may have been poorly sited, because the SPAC curve is cleaner on the small array circumferential (r2) data than on the radial (r1) data). Results are consistent with interpretations from a prior microtremor survey with a surface layer of $V_s < 200$ m/s and thickness 5m. The final S-wave velocity profile for Bolu is given in Figure 2.28 and Table 2.3.

Table 2.2: Layered-earth model at Düzce site from combined SPAC and HVSR modelling

Layer Number	Thickness (m)	Total Depth (m)	Vp (m/s)	Vs (m/s)	Vs error bounds	Rho (t/m ³)	
1	2	2	400	100	107-93	1.78	
2	4	6	400	200	212-184	1.8	
3	8	14	1500	235	242-222	2.0	
4	32	46	2000	400	430-360	2.14	
5	50	96	2000	600	720-490	2.14	
6	40	136	2000	650	nr	2.14	
7	200	336	2940	1000	±10%	2.39	Interpreted as base of Miocene sediments
8	400	736	2940	1150	nr	2.39	
9	1300	2036	2940	1300	nr	2.39	
10	0		4000	2250	±20%	2.8	
nr: not resolved							

An important point on depth of penetration is as follows; the low frequency limits from MMSPAC data correspond to 136m and 209m at Düzce and Bolu, respectively. The structure below these depths are obtained through HVSR analysis on microtremors which is presented in the next Chapter. For complement, the full velocity profile is presented here.

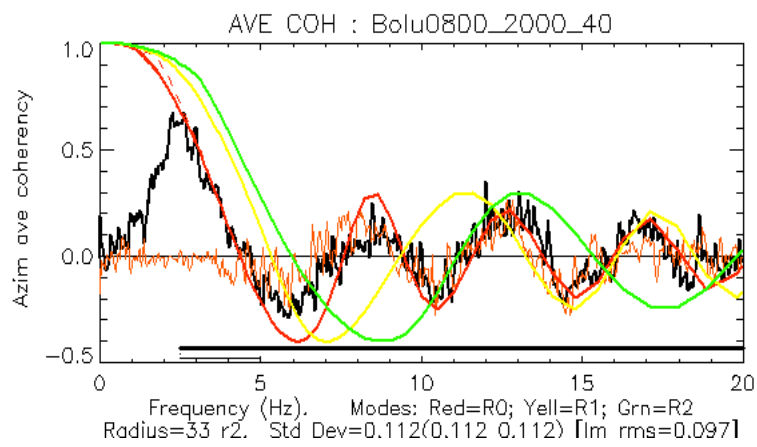
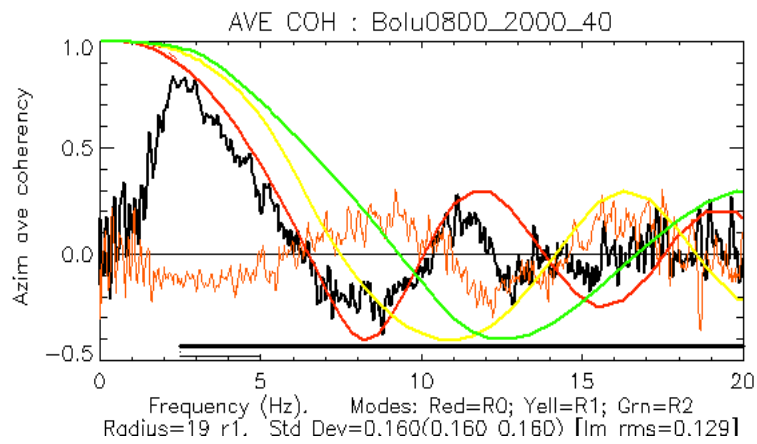


Figure 2.26: SPAC spectra at Bolu array (Top Panel: SPAC spectra for r1, Bottom Panel: SPAC spectra for r2)

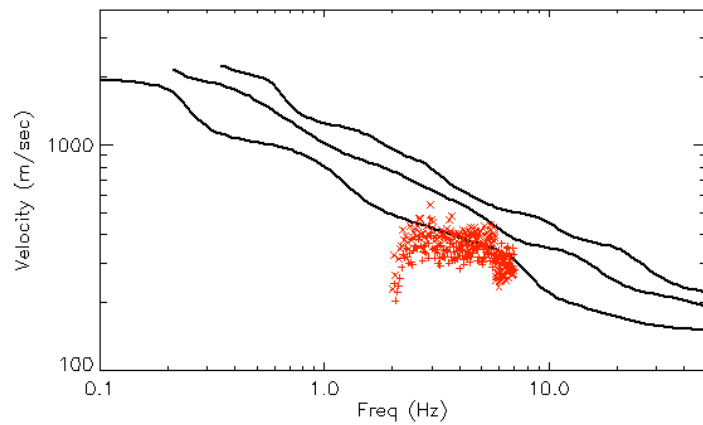


Figure 2.27: Dispersion curve at Bolu array (Black curves indicate theoretical dispersion curves whereas the red dots indicate observed dispersion)

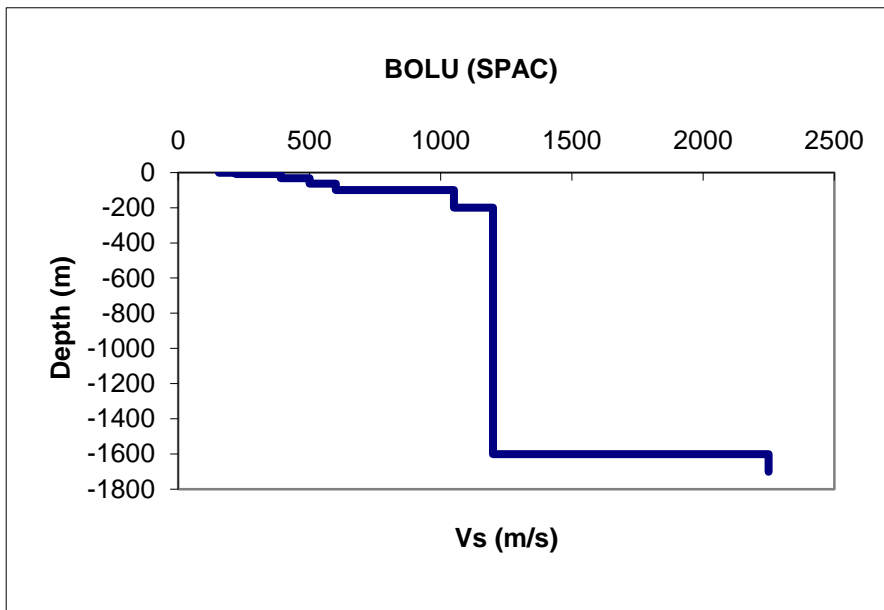


Figure 2.28: S-wave velocity profile at Bolu

Table 2.3: Layered-earth model at Bolu site from combined SPAC and HVSR modeling

Layer Number	Thickness (m)	Total Depth (m)	Vp (m/s)	Vs (m/s)	Vs error bounds	Rho (t/m ³)	
1	0.75	0.75	800	155	nr	1.78	
2	2	3	800	155	171-145	2.0	
3	2	5	1500	185	200-170	2.0	
4	8	13	2000	220	227-208	2.0	
5	32	45	2000	390	435-345	2.14	
6	64	109	2000	500	550-410	2.14	
7	100	209	2940	600	nr	2.14	
8	200	409	2940	900	±10%	2.39	Interpreted as base of Miocene sediments
9	200	609	2940	1050	nr	2.39	
10	1600	2209	4500	1200	nr	2.39	
11	0			2250	±20%	2.8	
nr: not resolved							

Figures 2.29 and 2.30 show the comparisons of the S-wave velocity profiles obtained in this thesis with those from previous studies. It is observed that MMSPAC method is more effective for the lower frequencies (deeper parts of the soil than the higher frequencies (shallow parts of the soil)). The S-wave velocity values from previous studies are 15-20% different for first 30 m depth due to frequency resolution of the MMSPAC method. In addition, for both Düzce and Bolu cities, MMSPAC method resolves deepest part of the soil with low frequency content effectively. Considering alternative methods for obtaining S-wave velocity, MMSPAC method has an advantage of simultaneously resolving the shallow, middle and deeper parts of the soil.

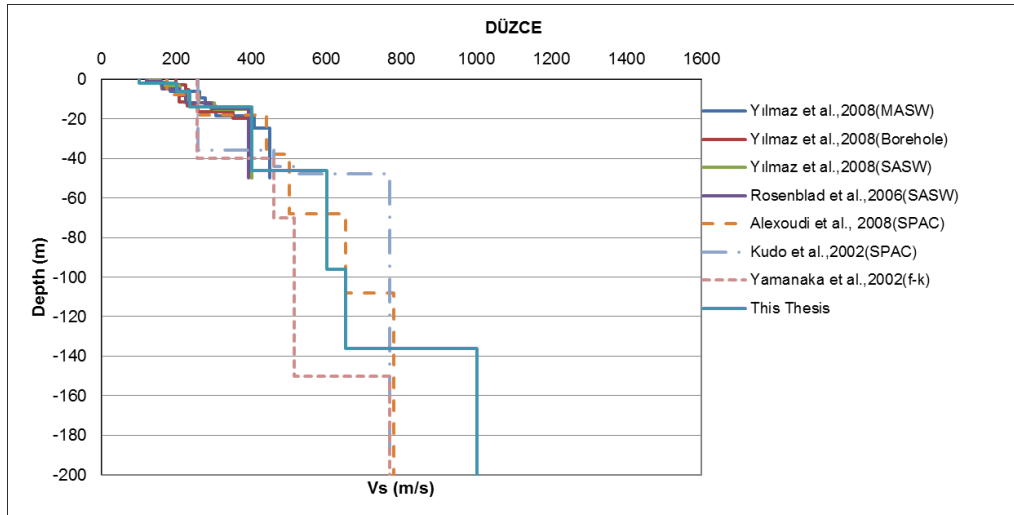


Figure 2.29: Comparison of the S-wave velocity profile obtained in this thesis with previous studies at Düzce site

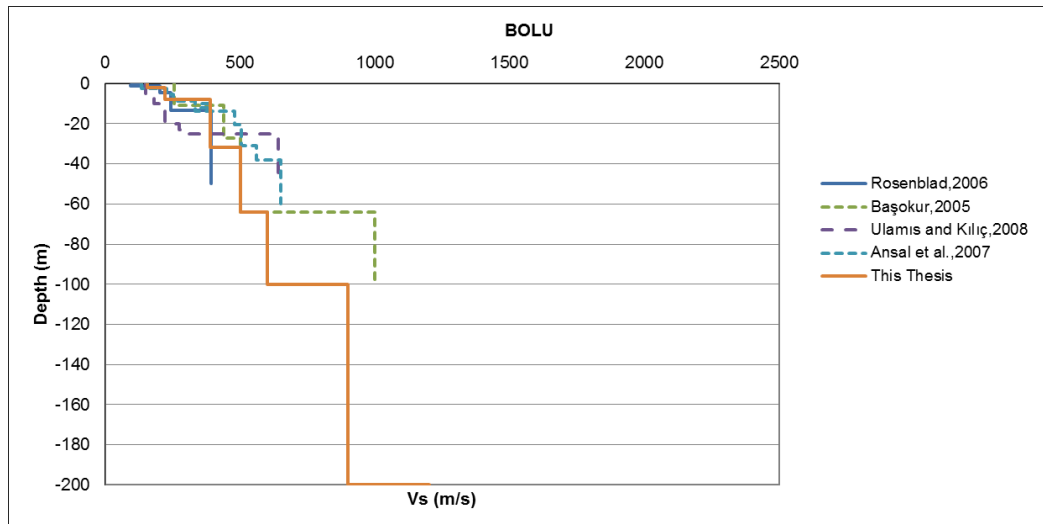


Figure 2.30: Comparison of the S-wave velocity profile obtained in this thesis with previous studies at Bolu site

In this chapter, one-dimensional S-wave velocity profiles are derived for Düzce and Bolu strong motion stations. These results will be used as input to the site response analysis in Chapter 3 to derive site amplifications.

Results of further applications of MMSPAC method on microtremor records from other regions in the world are presented in Appendix A.

CHAPTER 3

EVALUATION OF SITE RESPONSE BASED ON ALTERNATIVE METHODS

3.1 General

The main objective of this thesis is to compare the fundamental frequencies of soils and corresponding amplification factors from three alternative approaches which are HVSR with microtremor, HVSR with earthquake records and theoretical transfer functions. Comparative effectiveness of these techniques are assessed in sedimentary basins of Miocene age on the North Anatolian Fault zone. For this purpose, empirical Horizontal to Vertical Spectral Ratio based on microtremors, weak motions and strong motions are compared with one-dimensional theoretical transfer functions. The theoretical transfer functions are computed using S-wave velocity profiles inverted from microtremor data presented in the previous chapter.

HVSR method is performed for both microtremor and ground motion data recorded at two strong ground motion stations in Northwest Turkey. Weak and strong ground motions are analyzed separately for potential differences in the amplification factors and the fundamental frequencies. Then the S-wave profiles obtained from the microtremor analyses are employed in one-dimensional (1D) site response analyses. 1D site response modeling yields theoretical transfer functions at the sites of interest. Finally, results from alternative techniques are presented in the form of amplification factors and fundamental frequencies. Figure 3.1 displays the methods and data employed in this chapter.

3.2 Horizontal to Vertical Spectral Ratio Method

In the literature, a common empirical and practical method for evaluating local site phenomena is the Horizontal to Vertical Spectral Ratio method originally proposed by Nogoshi and Igarashi (1971) and Nakamura (1989). This method relies on the assumption that the vertical surface ground motion component is less amplified by the shallow soil layers than is the horizontal component. Single-station HVSR was originally applied on microtremor data (e.g.: Nakamura, 1989; Field and Jacob, 1993; Lermo and Chavez-Garcia, 1993; Huang and Teng, 1999; Rodriguez and Midorikawa, 2002) and is accepted commonly by the engineering community. Later research showed that it can also be employed effectively with earthquake data using S-wave portions of strong motion records. (e.g.: Lermo and Chavez-Garcia, 1993; Huang and Teng, 1999). Suzuki et al. (1995) demonstrated that HVSR from microtremors and strong ground motion have similar peak frequencies. Lachet and Bard (1994) argued that the HVSR from microtremors yields the correct resonance frequency while the corresponding amplitudes are not necessarily accurate.

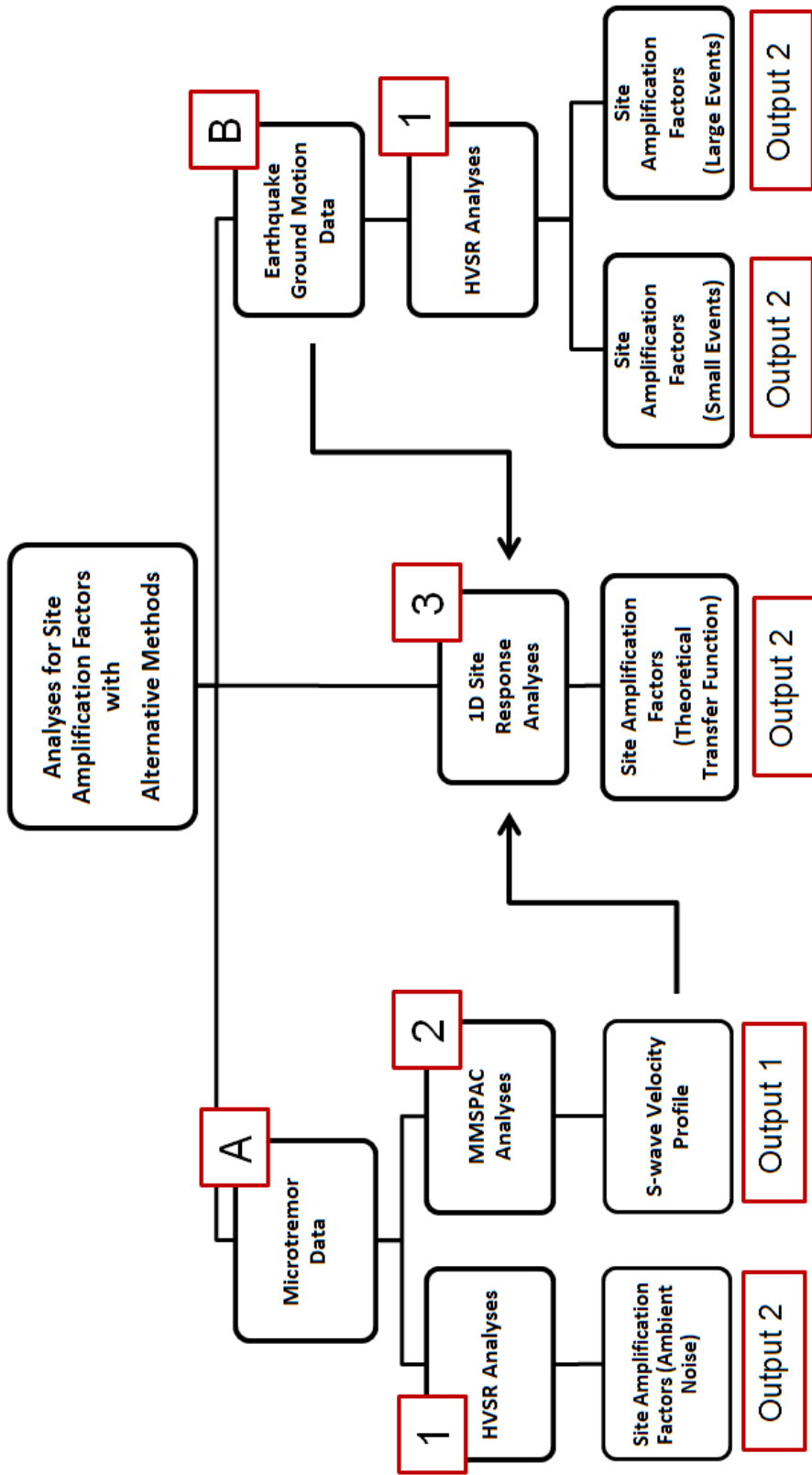


Figure 3.1: Flow chart displaying the analyses used in this chapter

However, there are other studies where HVSR amplitudes do correlate with site amplifications from other methods. For instance, Massa et al. (2004) found consistent results from HVSR based on both noise and earthquake records while evaluating local site amplifications in southern Italy.

The formulation of the HVSR method is explained following Lermo and Chavez (1993). Due to the negligible amplification effects in the vertical component, the source spectrum (A_s) can be calculated with vertical components of the motions as follows:

$$A_s = \frac{V_S}{V_B} \quad (3.1)$$

where V_S is the spectral amplitude of the vertical component of the motion at the surface and V_B is the spectral amplitude of the vertical component of the motion at the half-space (bedrock). An estimate of site effects is given as:

$$S_E = \frac{H_S}{H_B} \quad (3.2)$$

In Equation (3.2), H_S is the spectral amplitude of the horizontal component of the motion at the surface and H_B is the spectral amplitude of the horizontal component of the motion at the bedrock. To eliminate the source effects in S_E , modified site effect function S_M is calculated as:

$$S_M = \frac{S_E}{A_s} \quad (3.3)$$

Equation (3.3) is equivalent to the Equation (3.4)

$$S_M = \frac{\frac{H_S}{H_B}}{\frac{V_S}{V_B}} \quad (3.4)$$

Then, if the ratio H_B/V_B is assumed to be 1, the site effect function can be written as:

$$S_M = \frac{H_S}{V_S} \quad (3.5)$$

3.2.1 HVSR Analyses of Microtremor Data

The microtremor data measured at stations Düzce and Bolu presented in Chapter 2 are used herein. To summarize, in Düzce, two nested four-station equilateral triangular arrays with side-lengths 30m and 90m are employed whereas in Bolu, a single four-station triangular array of side-length 33.3m is employed. A typical four-station triangular array is displayed in Figure 3.2. For microtremor measurements; Guralp CMG6TD seismometers containing internal data recorders are used. The sampling rate is 100 Hz.

To calculate HVSR spectra, data segments are used with a typical duration of 20 minutes at the stations. HVSR spectra at Düzce and Bolu are computed simply by dividing the Fourier amplitudes of the mean horizontal component to that of the vertical component.

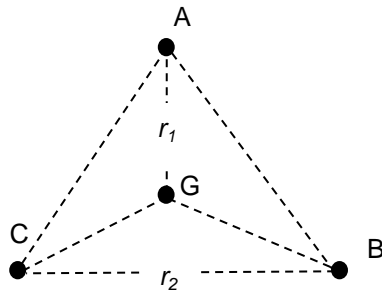


Figure 3.2: A typical four-station equilateral triangular array used for microtremor measurements in this study (A, B, C and G indicate the seismometer locations; r_1 and r_2 are the inter-station separations)

The HVSR obtained from microtremors at Düzce and Bolu are displayed in Figure 3.3 and 3.4.

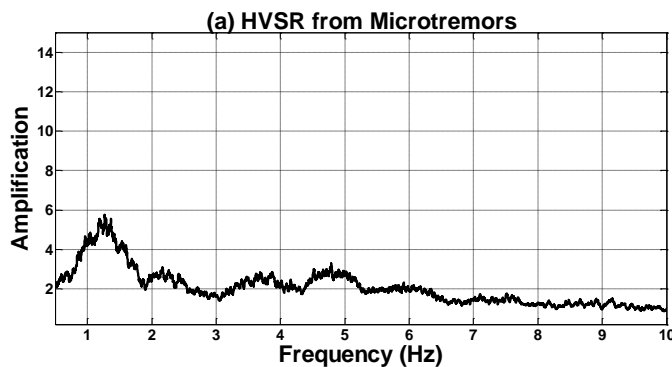


Figure 3.3: HVSR from microtremors at Düzce

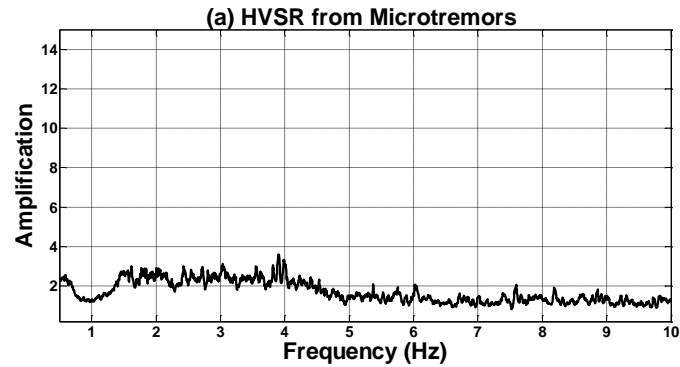


Figure 3.4: HVSr from microtremors at Bolu

3.2.2 HVSr Analyses of Earthquake Data

Main steps of the HVSr analysis based on ground motion data are demonstrated in Figure 3.5. The analysis of each ground motion record starts with the picking of the S-wave portion manually and computing the Fourier Amplitude Spectrum (FAS) of the horizontal and vertical components of the motion. Then, the average FAS of the two horizontal components is divided by FAS of the vertical component. A Hann filter of 0.4 Hz-bandwidth is performed to smooth the computed spectra.

For the HVSr analyses based on strong ground motions, data from past events recorded at Düzce and Bolu are used. The records are obtained from the webpage of the Strong Ground Motion Database of Turkey (via <http://daphne.deprem.gov.tr>). In previous studies, it was demonstrated that HVSr can systematically identify nonlinear site effects based on the significant differences observed in H/V ratios of weak and strong motions (e.g.: Wen et al., 1994). Similarly, in this section of the thesis, a further comparison is made between events that generated weak motions ($M_w \leq 4.0$ and Peak Ground Acceleration (PGA) ≤ 0.015 g) and strong motions ($M_w > 7.0$ and $PGA > 0.2$ g) at the two stations with the objective of evaluating any potential differences in the spectral ratios. It must be noted that the term “weak motion” mostly refers velocity data from broadband seismometers. But, as explained within the content of this thesis “weak motions” refer to acceleration records with low amplitude.

The epicentral distances of these events from the stations are within the range of 10-50 km. Information on the weak motion records measured at Düzce and Bolu stations are displayed in Tables 3.1 and 3.2. For Düzce, 31 weak motion records are used whereas 25 weak motion records are used for Bolu to compute the mean HVSrs at these stations. There are only two earthquakes that generated motions with $M_w > 7.0$ and $PGA > 0.2$ g; the 17 August 1999 Kocaeli ($M_w = 7.4$) and the 12 November 1999 Düzce ($M_w = 7.2$) events. Thus, the comparison between the HVSr from weak motions and the HVSr from these two main-shock records are performed in this section. There are two objectives for this comparison: first, to see if empirical HVSr curves based on records from large events can estimate resonance frequencies at a soil site, and second to observe any differences that can be attributed to nonlinear effects.

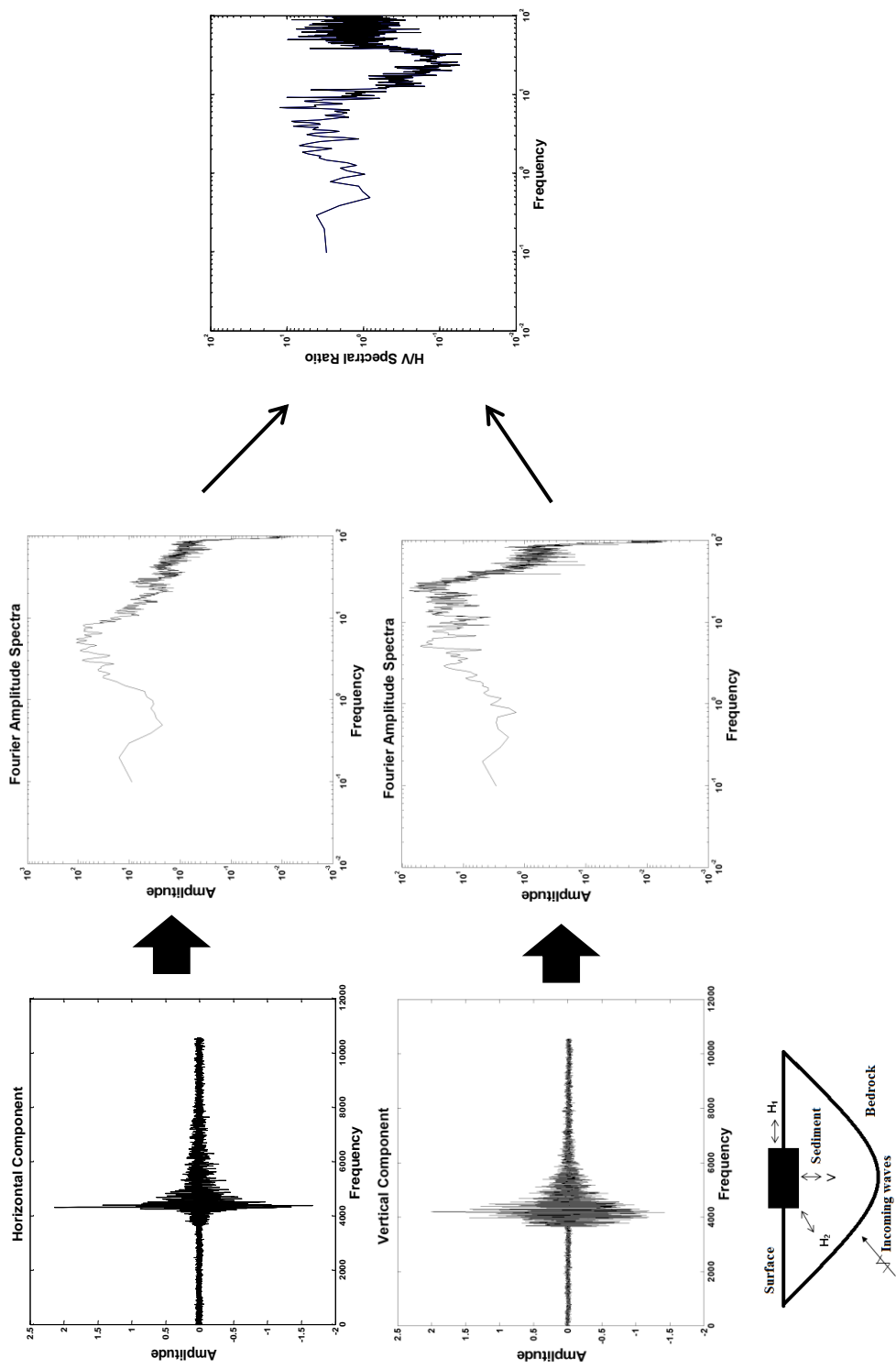


Figure 3.5: Main steps of HVSR method with ground motion data

Table 3.1: Information on the ground motion records (with $PGA < 0.015\text{ g}$) recorded at station Düzce

Record ID	Event ID (as given on the database web page)	Magnitude (Mw)	N-S PGA (cm/sec^2)	E-W PGA (cm/sec^2)	U-D PGA (cm/sec^2)	R_{epi} (km)
1	20030701143320_8101	3.2	0.76	2.9	1.5	13.84
2	20000518054600_8101	2.9	0.92	0.4	0.61	24.51
3	20000720045046_8101	2.9	1.01	1.25	0.58	19.67
4	20000622215935_8101	2.9	1.07	1.31	3.27	4.2
5	20000615163625_8101	2.5	1.1	2.11	0.7	16.2
6	20010915071042_8101	2.7	1.19	2.93	1.22	16.34
7	20000530115801_8101	2.8	1.22	1.59	0.82	14.07
8	20010424234526_8101	2.9	1.34	0.98	0.7	15.29
9	20010410202427_8101	3.2	1.37	1.37	1.37	11.91
10	20030308111824_8101	3.8	1.37	1.77	1.13	49.15
11	20000519013112_8101	2.6	1.43	1.77	1.07	9.58
12	20011004213753_8101	2.9	1.56	1.86	1.25	14.51
13	20000830202142_8101	3.2	1.62	1.62	3.14	13.41
14	20040913014845_8101	3.7	1.74	1.98	1.5	19.06
15	20040413214740_8101	4.6	1.95	2.87	1.01	39.96
16	20000323073912_8101	3.2	2.14	2.05	2.16	19.48
17	20000615124752_8101	3	2.17	3.97	1.07	19.79
18	20000614045331_8101	3.7	2.26	3.05	2.53	14.6
19	20000327110251_8101	3.8	2.33	2.83	1.98	33.39
20	20020110212154_8101	3.2	2.38	2.9	2.59	16.23
21	20020104204422_8101	3.4	2.63	3.57	1.59	21.91
22	20000322144913_8101	4	2.83	2.56	4.71	13.67
23	20010418210611_8101	3.7	2.99	3.66	2.29	22.17
24	20040816183913_8101	3.3	3.57	2.66	1.5	22.2
25	20070206010333_8101	3.6	3.66	3.75	1.74	21.9
26	20000709032249_8101	3.4	4.24	3.33	2.81	18.04
27	20030527232536_8101	3.9	6.5	4.88	12.15	15.91
28	20030527214821_8101	3.7	7.9	7.11	7.51	12.56
29	20000105141007_8101	4.4	9	15.42	7.64	7.52
30	20061017194040_8101	3.5	10.47	5.8	4.24	7.05
31	20020826224407_8101	3.7	14.62	10.62	5.68	14.54

Table 3.2: Information on the ground motion records (with PGA<0.015 g) recorded at station Bolu

Record ID	Event ID (as given on the database web page)	Mw	North-South PGA (cm/sec ²)	East- West PGA (cm/sec ²)	Up-Down PGA (cm/sec ²)	R _{epi} (km)
1	20000707001619_1401	4.2	0.69	0.84	0.29	196.3
2	20010616063327_1401	2.7	1.02	1.38	0.7	15.9
3	20000402185740_1401	4.5	1.13	1.29	0.89	111.5
4	20000327110251_1401	3.8	1.24	0.84	0.57	73.24
5	20000215192358_1401	2.7	1.34	0.72	0.99	34.45
6	20000215210356_1401	2.9	1.42	0.55	0.78	20.99
7	20000822114026_1401	4.8	1.5	1.19	0.83	67.01
8	20010322140248_1401	4.6	1.55	1.19	0.74	121.0
9	20000214222959_1401	3.4	1.61	0.81	0.69	18.85
10	20000216191446_1401	3.3	2.14	1.95	2.01	17.88
11	20000216053016_1401	3.4	2.33	2.21	0.9	22.42
12	19990820100035_1401	4.4	3.54	3.36	2.08	85.85
13	20001113031242_1401	4.1	4.22	3.12	1.13	70.44
14	20010709225243_1401	3	4.44	1.71	2.64	5.64
15	20000331130444_1401	3.7	5.65	4.34	6.24	29.08
16	19991112231100_1401	4	6.33	7.7	7.79	18.67
17	19990820155919_1401	4.4	6.41	5.31	1.16	70.24
18	19991112182453_1401	4.7	7.65	1.39	3.77	22.73
19	19991113025900_1401	4.2	7.78	5.42	7.74	44.6
20	19991112224908_1401	4.2	8.03	6.49	7.78	47.08
21	20000823134129_1401	5.4	9.62	9.79	5.75	71.67
22	19991112175735_1401	4.8	11.24	10.45	4.43	13.03
23	19991112172305_1401	5.1	12.47	7.38	3.43	37.81
24	19991220032728_1401	4.1	13.41	7.02	7.78	55.47
25	19991112174658_1401	4.8	14.36	3.76	7.78	54.38

Figures 3.6 and 3.7 display the HVSR spectra from weak and strong ground motions at Düzce and Bolu, respectively. Remarks and observations on these HVSR curves will be discussed in detail in Section 3.4.

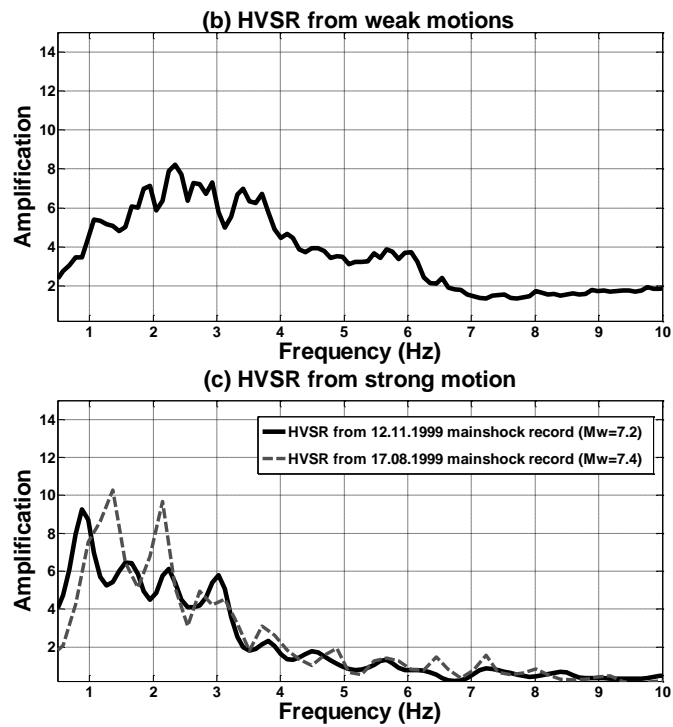


Figure 3.6: HVSr spectra from weak (a) and strong (b) ground motion at Düzce

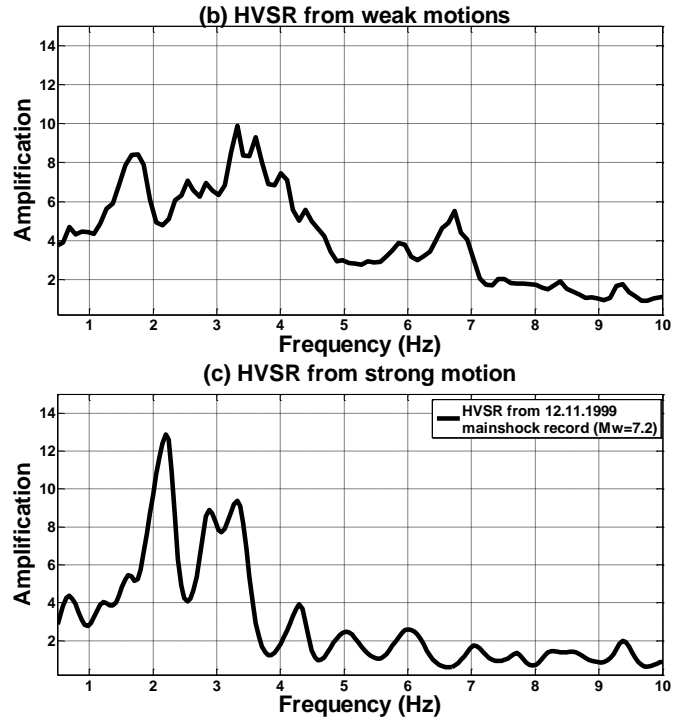


Figure 3.7: HVSr spectra from weak (a) and strong (b) ground motion at Bolu

3.3 One-Dimensional Site Response Modeling

One of the commonly employed methods in geotechnical engineering for computing site amplifications is one-dimensional site response modeling. One-dimensional site response modeling is used to predict the surface ground motions, to generate design response spectrum, to assess dynamic stresses and strains for determining liquefaction hazards and to calculate earthquake-induced forces (Kramer, 1996). One-dimensional site response analysis is performed with SHAKE, a very common computer program that computes the theoretical transfer function of a soil profile in the frequency domain (Schnabel et al., 1972)

3.3.1 Theory of One-Dimensional Site Response Analysis

One-dimensional site response modeling is based on the assumption that all boundaries of the surface soil layers are horizontal and that soil response is caused by SH waves propagating in vertical direction. It is also assumed that layers of the soil and bedrock extend infinitely in the horizontal direction (Kramer, 1996). These aforementioned assumptions are shown in Figure 3.8.

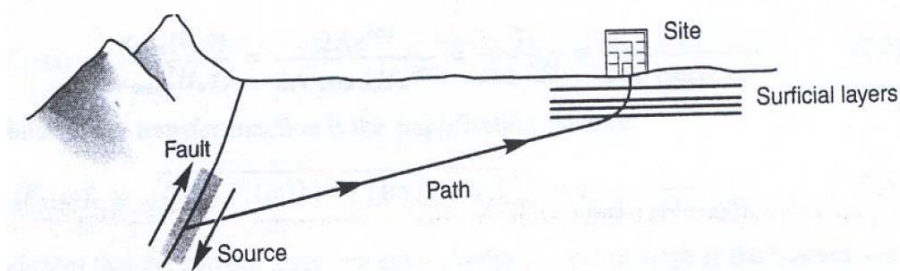


Figure 3.8: Refraction process (Figure is adapted from Kramer, 1996)

Description of the terms used in the analysis is necessary to understand site response modeling. In Figure 3.9 (a), motion at the soil layer surface is called free surface motion whereas the motion at base of the soil layer is called bedrock motion. The motion at a location where bedrock is exposed at the ground surface is called a rock outcropping motion. If the soil deposit was not present (Figure 3.9 (b)), the motion at the top of the bedrock would be the bedrock outcropping motion.

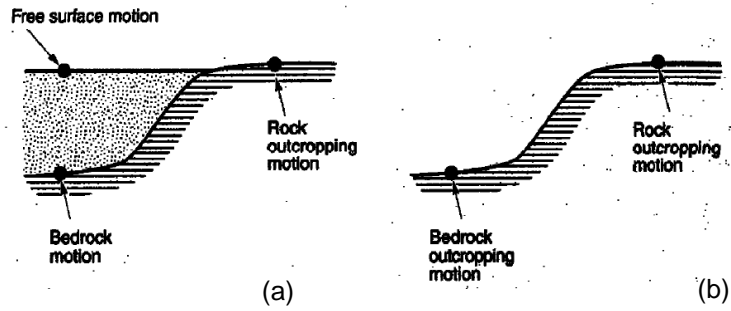


Figure 3.9: Description of terms used in analysis (Kramer, 1996)

One dimensional site response modeling is performed with the computer program SHAKE (Schnabel et al., 1972). The following section describes theory of the analysis performed. Next, the theory is discussed in two groups with respect to number of the soil layers: single soil layer and multiple soil layers.

a) Single soil layer

Figure 3.10 shows a profile that consists of an elastic layer of rock beneath a uniform soil layer. Horizontal displacement due to the vertical propagation of the harmonic S-wave is written as (Kramer, 1996):

$$u_s(z_s, t) = A_s e^{i(\omega t + k_s^* z_s)} + B_s e^{i(\omega t - k_s^* z_s)} \quad (3.5)$$

$$u_r(z_r, t) = A_r e^{i(\omega t + k_r^* z_r)} + B_r e^{i(\omega t - k_r^* z_r)} \quad (3.6)$$

where the subscripts r and s indicate rock and soil, respectively. Here, ω is the circular frequency of ground shaking, k is the wave number ($= \omega/V_s$), A and B are amplitudes of the waves traveling in $-z$ and z directions, respectively.

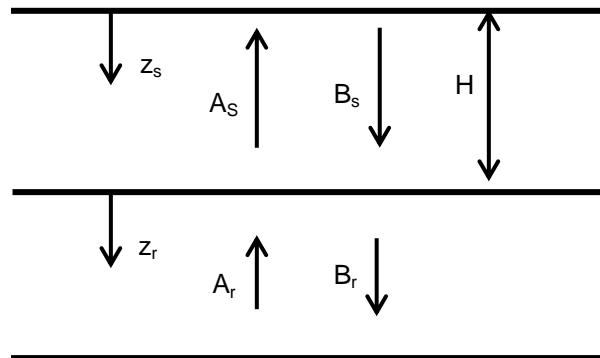


Figure 3.10: Illustration of a single layer of soil on an elastic rock

Shear stress τ is zero at the ground surface ($z_s = 0$). Thus:

$$\tau(0, t) = G_s^* \gamma(0, t) = G_s^* \frac{\partial u_s(0, t)}{\partial z_s} = 0 \quad (3.7)$$

where $G_s^* = G(1 + 2i\xi)$ indicates the complex shear modulus and ξ is the damping ratio of the soil. Substituting Equation (3.5) and Equation (3.7) and differentiating yields:

$$G_s^* i k_s (A_s e^{ik_s(0)} - B_s e^{-ik_s(0)}) e^{i\omega t} = G_s^* i k_s (A_s - B_s) e^{i\omega t} = 0 \quad (3.8)$$

Equation (3.8) is correct when $A_s = B_s$. Compatibility of displacement and continuity of stresses at boundary between the soil and rock require:

$$u_s(z_s = H) = u_r(z_r = 0) \quad (3.9)$$

$$\tau_s(z_s = H) = \tau_r(z_r = 0) \quad (3.10)$$

Substituting Equations (3.5) and (3.6) into Equation (3.9):

$$A_s (e^{ik_s^* H} + e^{-ik_s^* H}) = A_r + B_r \quad (3.11)$$

From Equation (3.10) and shear stress definition $\tau = G_s^* \frac{\partial u}{\partial z}$

$$A_s i G_s^* k_s^* (e^{ik_s^* H} - e^{-ik_s^* H}) = i G_r^* k_r^* (A_r - B_r)$$

or

$$\frac{G_s^* k_s^*}{G_r^* k_r^*} A_s (e^{ik_s^* H} - e^{-ik_s^* H}) = (A_r - B_r) \quad (3.12)$$

So the ratio becomes:

$$\frac{G_s^* k_s^*}{G_r^* k_r^*} = \alpha_z^*$$

where α_z^* indicates the ratio of the complex impedance. Solving Equations (3.11) and (3.12)

$$A_r = \frac{1}{2} A_s [(1 + \alpha_z^*) e^{ik_s^* H} + (1 - \alpha_z^*) e^{-ik_s^* H}] \quad (3.13)$$

$$B_r = \frac{1}{2} A_s [(1 - \alpha_z^*) e^{ik_s^* H} + (1 + \alpha_z^*) e^{-ik_s^* H}] \quad (3.14)$$

If a vertical propagating shear wave of amplitude A , traveled upward through the rock and the soil was not present, the free surface effect at the rock outcrop would produce a bedrock outcropping motion of amplitude $2A$. If the soil was present, the free surface motion amplitude would be

$$A_s = \frac{4A}{2(1 + \alpha_z^*) e^{ik_s^* H} + (1 - \alpha_z^*) e^{-ik_s^* H}} \quad (3.15)$$

Finally, the transfer function $F(\omega)$ can be calculated with Equation (3.16). $F(\omega)$ is the ratio of the soil surface amplitude to rock outcrop amplitude.

$$F(\omega) = \frac{2}{(1 + \alpha_z^*)e^{ik_s^* H} + (1 - \alpha_z^*)e^{-ik_s^* H}} \quad (3.16)$$

The complex transfer function can be also written with Euler's law as:

$$F(\omega) = \frac{2}{\cos k_s^* H + i \alpha_z^* \sin k_s^* H} \quad (3.17)$$

b) Multiple Soil Layers

The horizontal displacement for layer j is computed as follows:

$$u_j(z_j, t) = (A_j e^{ik_j^* z_j} + B_j e^{-ik_j^* z_j}) e^{i\omega t} \quad (3.18)$$

Compatibility of displacement at the boundary between layer j and layer j+1 is expressed as:

$$A_{j+1} + B_{j+1} = A_j e^{ik_j^* h_j} + B_j e^{-ik_j^* h_j} \quad (3.19)$$

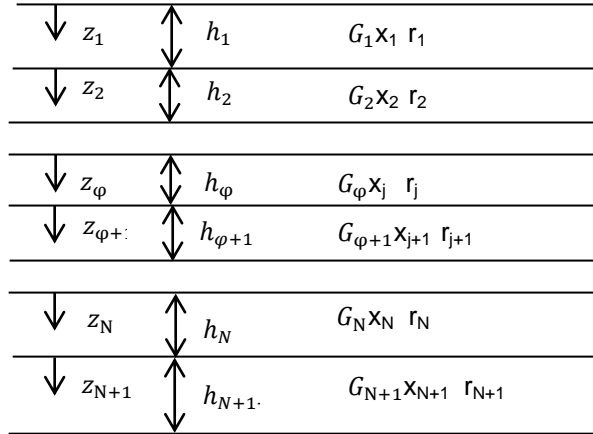


Figure 3.11: Illustration of a layered soil deposit on elastic rock

And continuity of shear stresses requires that

$$A_{j+1} - B_{j+1} = \frac{G_j^* k_j^*}{G_{j+1}^* k_{j+1}^*} (A_j e^{ik_s^* h_j} - B_j e^{-ik_s^* h_j}) \quad (3.20)$$

It should be noted that Equations (3.19) and (3.20) for multiple soil profiles replace Equations (3.11) and (3.12) for single layer soil profiles. In Equation (3.21), α_j^* indicates the complex

impedance ratio between layers j and j+1. The wave amplitudes for layer j+1 can be computed from amplitudes of layer j by solving Equations (3.19) and (3.20):

$$A_{j+1} = \frac{1}{2} A_j (1 + \alpha_j^*) e^{ik_j^* h_j} + \frac{1}{2} B_j (1 - \alpha_j^*) e^{-ik_j^* h_j} \quad (3.21)$$

$$B_{j+1} = \frac{1}{2} A_j (1 - \alpha_j^*) e^{ik_j^* h_j} + \frac{1}{2} B_j (1 + \alpha_j^*) e^{-ik_j^* h_j} \quad (3.22)$$

At the surface ($z_1 = 0$), the shear stress is zero which means $A_1 = B_1$. Applying Equations (3.21) and (3.22) for $j=1,2,3,\dots,N$, the coefficient A_{j+1} and B_{j+1} can be related to A_j and B_j by:

$$A_{j+1} = a_{j+1}(\omega) A_1 \quad (3.23)$$

$$B_{j+1} = b_{j+1}(\omega) B_1 \quad (3.24)$$

where the function a_{j+1} and b_{j+1} indicate the effects of the wave interactions that take place at all of the layer interfaces. Finally, the transfer function can be computed as:

$$F_{ij}(\omega) = \frac{a_i(\omega) + b_i(\omega)}{a_j(\omega) + b_j(\omega)} \quad (3.25)$$

c) Equivalent Linear Analysis

Modeling the nonlinear stress-strain behavior of soft soils is a very significant research problem in geotechnical engineering. However, this complex behavior cannot be fully modeled in SHAKE analyses because the calculation of the transfer functions relies on the superposition principles that are only valid for linear systems. Still, the nonlinear soil response can be approximated with an equivalent linear approach.

In this approach, analyses assume the secant shear modulus as the dynamic shear modulus. While the shear strain level increases, the corresponding secant shear modulus reduces. The relationship between secant shear modulus and shear strain amplitude is defined by a modulus reduction curve. SHAKE models the damping of soil layers with an equivalent viscous damping. Similar to the modulus reduction curve, there is also a damping curve for every soil layer that defines the relationship between the equivalent damping ratio and shear strain.

An equivalent linear analysis starts with an initially assumed value of shear strain, the corresponding shear modulus, and damping ratios. After the first iteration, the effective shear strain is defined as:

$$\gamma_{\text{eff}} = R_\gamma \gamma_{\text{max}} \quad (3.26)$$

where R_γ is the strain reduction factor. SHAKE assumes that:

$$R_\gamma = \frac{M - 1}{10} \quad (3.27)$$

where M is the moment magnitude of the event that the records belongs to.

In the next iteration, shear modulus and damping ratio corresponding to γ_{eff} is utilized. The computations are repeated until the calculated effective strain remains almost constant from one iteration to the next. The equivalent linear analysis is assumed to have converged when effective strain does not vary any more at each iteration.

3.3.2 Implementation of One-Dimensional Site Response Modeling

In SHAKE program the soil is modeled as a series of infinite horizontal layers on top of uniform half-space where the non-linear behavior of the soil is simulated with an equivalent linear analysis. The input parameters required are thickness, density, wave velocity, shear modulus reduction, plasticity index (PI) and damping curves of each layer. The geotechnical information for the stations along with detailed borehole logs is available on the web page for Turkish National Strong Ground Motion Network (<http://daphne.deprem.gov.tr>). For the wave velocities, 1D shear-wave velocity models obtained from the MMSPAC analyses are employed. The corresponding input parameters for soil profiles at Düzce and Bolu are displayed in Tables 3.3 and 3.4.

As explained before, site response analyses require ground motion records as input at the bedrock level yielding the surface acceleration and the transfer function as outputs. Since the soil layers are assigned viscoelastic properties, the results depend on the amplitude of the input accelerograms. In this study, two different ground motion records are used as input to the SHAKE analyses; first is a weak motion record with a PGA of 0.003g measured at a rock station in Northwestern Turkey (Station SKR in Sakarya) and second is from the 17 August 1999 Kocaeli (Mw=7.4) mainshock with a PGA of 0.4g, also recorded at SKR.

The transfer functions for these two accelerograms are computed and displayed in Figures 3.12 and 3.13 for Düzce and Bolu stations, respectively.

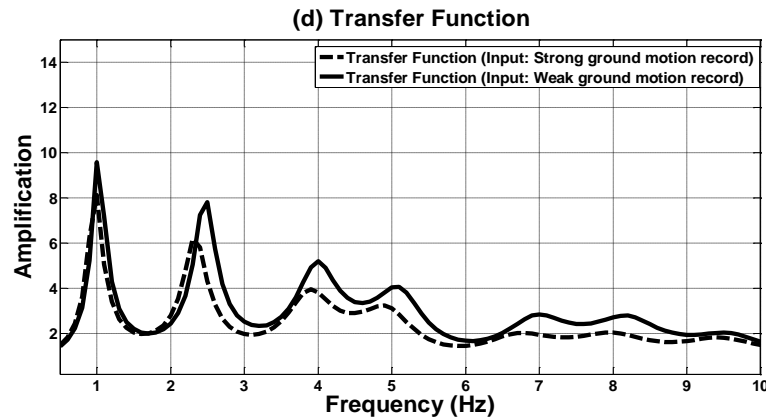


Figure 3.12: Transfer function at Düzce

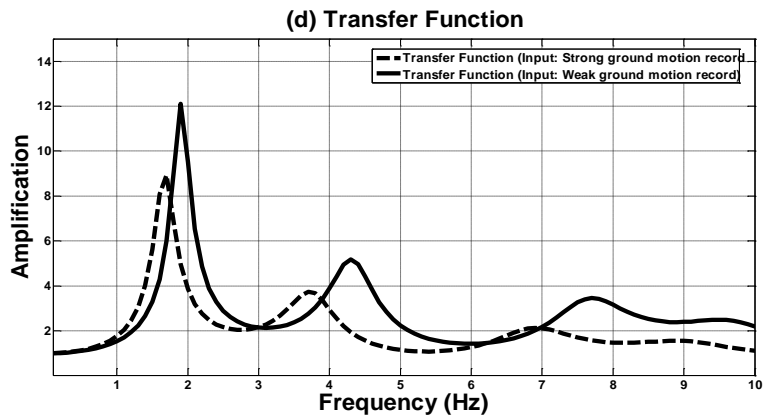


Figure 3.13: Transfer function at Bolu

Table 3.3: Geotechnical and geophysical parameters of the soil layers at Düzce site

Layer Number	Material Type	H (m)	Vs (m/s)	Modulus Curve	Damping Curve
1	Filling	2	100	Linear	Linear
2	Clay	4	200	Clay - PI=10-20 (Sun et al.)	Clay – Lower Bound (Sun et al.)
3	Clay	8	235	Clay - PI=20-40 (Sun et al.)	Clay - Average (Sun et al.)
4	Sand	32	400	Sand (Seed & Idriss) - Average	Sand (Seed & Idriss) - Average
5	Sand	50	600	Sand (Seed & Idriss) - Average	Sand (Seed & Idriss) - Average
6	Sand	40	650	Sand (Seed & Idriss) - Average	Sand (Seed & Idriss) - Average
7	Rock	Infinite	1000	Rock	Rock

Table 3.4: Geotechnical and geophysical parameters of the soil layers at Bolu site

Layer Number	Material Type	H (m)	Vs (m/s)	Modulus Curve	Damping Curve
1	Filling	0.75	155	Linear	Linear
2	Sandy-Clay	2	155	Clay - PI=20-40 (Sun et al.)	Clay - Average (Sun et al.)
3	Clay	2	185	Clay - PI= 40-80 (Sun et al.)	Clay – Upper Bound (Sun et al.)
4	Silty- Clay	8	220	Clay - PI=10-20 (Sun et al.)	Clay - Lower Bound (Sun et al.)
5	Clay	32	390	Clay - PI=20-40 (Sun et al.)	Clay - Average (Sun et al.)
6	Clay	64	500	Clay - PI=20-40 (Sun et al.)	Clay - Average (Sun et al.)
7	Rock	Infinite	900	Rock	Rock

In the literature, there are correlations between Vs and Standard Penetration Test (SPT) values. However, estimates of Vs from these conversions are always approximate. Thus, in this thesis Vs profile from MMSPAC is used.

3.4 Comparison of Results from Alternative Techniques

The differences in the amplification curves from alternative methods are investigated for each station separately. Figure 3.14 compares the results in terms of HVSR from microtremors, mean HVSR from weak motion records, HVSR from strong motion records and theoretical transfer functions for Düzce. The HVSR curve based on microtremors indicates a fundamental frequency of 1.2 Hz corresponding to an amplification factor around 6 (Figure 3.14.a). On the same curve, there is a second peak between 2 and 2.5 Hz with a lower amplification ratio (around 3) corresponding to the second mode. There are two other smaller peaks around 4 Hz and 5 Hz. HVSR curve from weak motion records shown in Figure 3.14.b confirms the fundamental frequency obtained from microtremors as well as the corresponding amplification factor. Other clear peaks around 2.5 Hz and 3.5 Hz are also observed on the HVSR from weak motion records. The single-record strong motion HVSR from the Düzce record of the 17 August 1999 Kocaeli event yields the same fundamental frequency (around 1.2 Hz) that the weak motion and microtremor HVSR curves indicate (Figure 3.14.c). However, the amplification factor from this strong motion record corresponding to the fundamental frequency overestimates the values from the previous curves by a factor of 1.5. The HVSR curve from the Düzce strong-motion record of the 12 November 1999 Düzce event is slightly shifted to lower frequencies yielding a lower fundamental frequency around 0.9 Hz. This curve shows approximately 10% lower amplitudes when compared to the HVSR from the Düzce record of the 17 August 1999 event. This observation could indicate potential nonlinearity of the soil at Düzce for the 12 November 1999 event where Düzce was located only 9 km away from the epicenter with a PGA of 0.5g. Figure 3.14.d shows that the theoretical transfer functions computed in SHAKE are in close agreement with the first and higher order modal frequencies obtained from microtremors. For the fundamental frequency, the theoretical curves from both weak and strong motions are the same as the frequency obtained from microtremor HVSR. For the higher modes, the transfer function from a strong ground motion input is slightly shifted to the lower frequencies with lower amplitudes when compared to the transfer function computed

using a weak motion record. This is expected as a consequence of the inelastic soil modeling implying nonlinearity of the soil due to the strong motion record. In addition, the amplitudes from transfer functions exceed the observed amplitudes from microtremors by a factor of 1.5 for the fundamental frequency, although for the higher modes, the difference is smaller. On the other hand, the amplification factors from the theoretical analysis are consistent with those observed from both weak and strong motion HVSR. Finally, at Düzce, for the higher modes, all empirical HVSR curves tend to give similar peak frequencies and consistent amplification values.

Figure 3.15 shows the corresponding comparisons for Bolu. The HVSR from microtremors at Bolu does not show peaks as distinctive as those at Düzce. Nevertheless, there are two subtle peaks at around 1.5 to 2 Hz and 4 Hz. The HVSR based on weak motions yields local peaks consistent in frequency with the microtremors (at 1.8 Hz, and 3.5 Hz) although with larger amplification factors. There is no strong motion record available at Bolu from the 17 August 1999 Kocaeli mainshock, but the strong motion record from the 12 November 1999 Düzce mainshock yields an interesting result. The fundamental frequency is around 2 Hz which is slightly higher than that observed with weak motion HVSR. On the other hand, the frequency corresponding to the second peak obtained from the mainshock record is consistent with those observed on microtremor and weak motion records. Interestingly, when the theoretical transfer functions at Bolu are compared with the HVSR curve from strong motions (Figures 3.15.c and 3.15.d), we observe consistent results in terms of fundamental frequencies (around 2 Hz) and the corresponding amplification factors (around 12).

Finally, it should be noted that at both stations, amplification factors from transfer functions are found to be closer to those observed on mean HVSR from weak motions and the single strong motion records.

Further detailed conclusions are expressed in the next chapter.

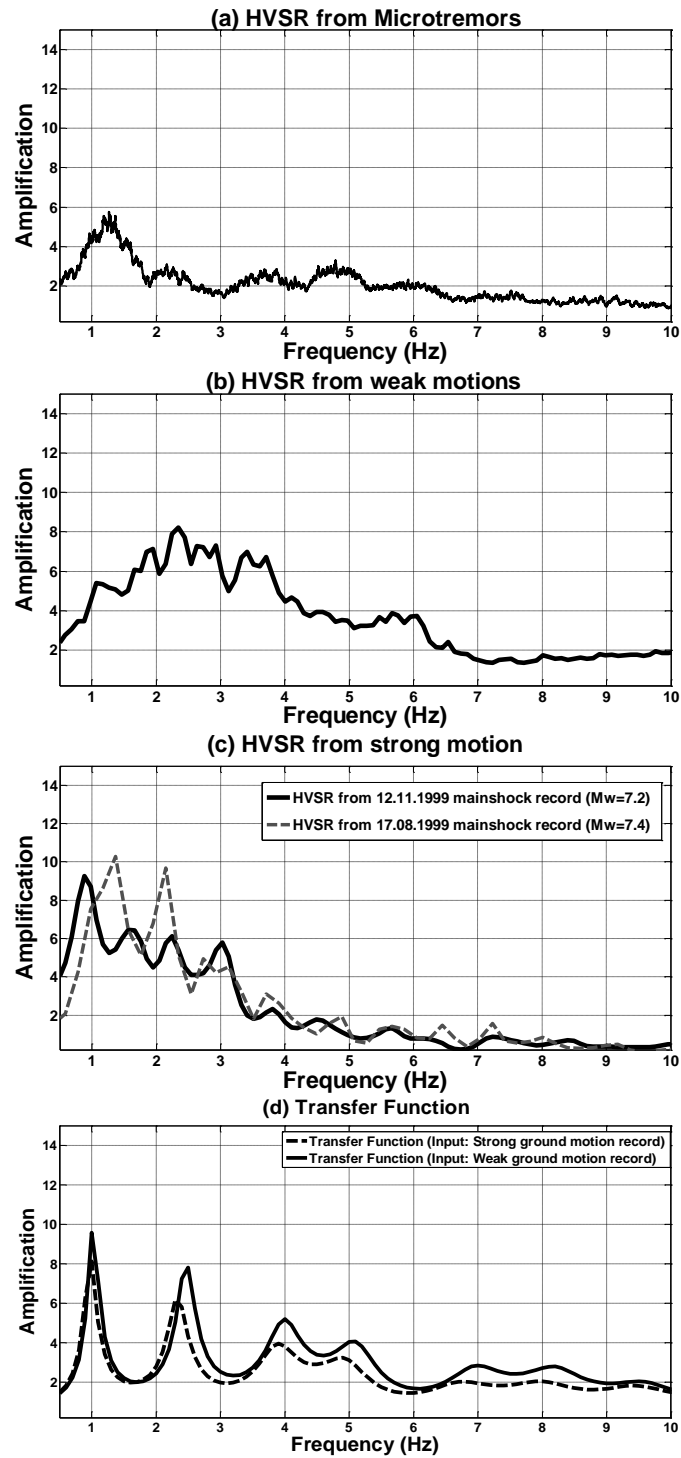


Figure 3.14: Comparison of amplification spectra at Düzce in terms of (a) HVSr from microtremors, (b) HVSr from weak motions, (c) HVSr from 1999 Kocaeli and 1999 Düzce mainshocks, (d) Theoretical transfer functions

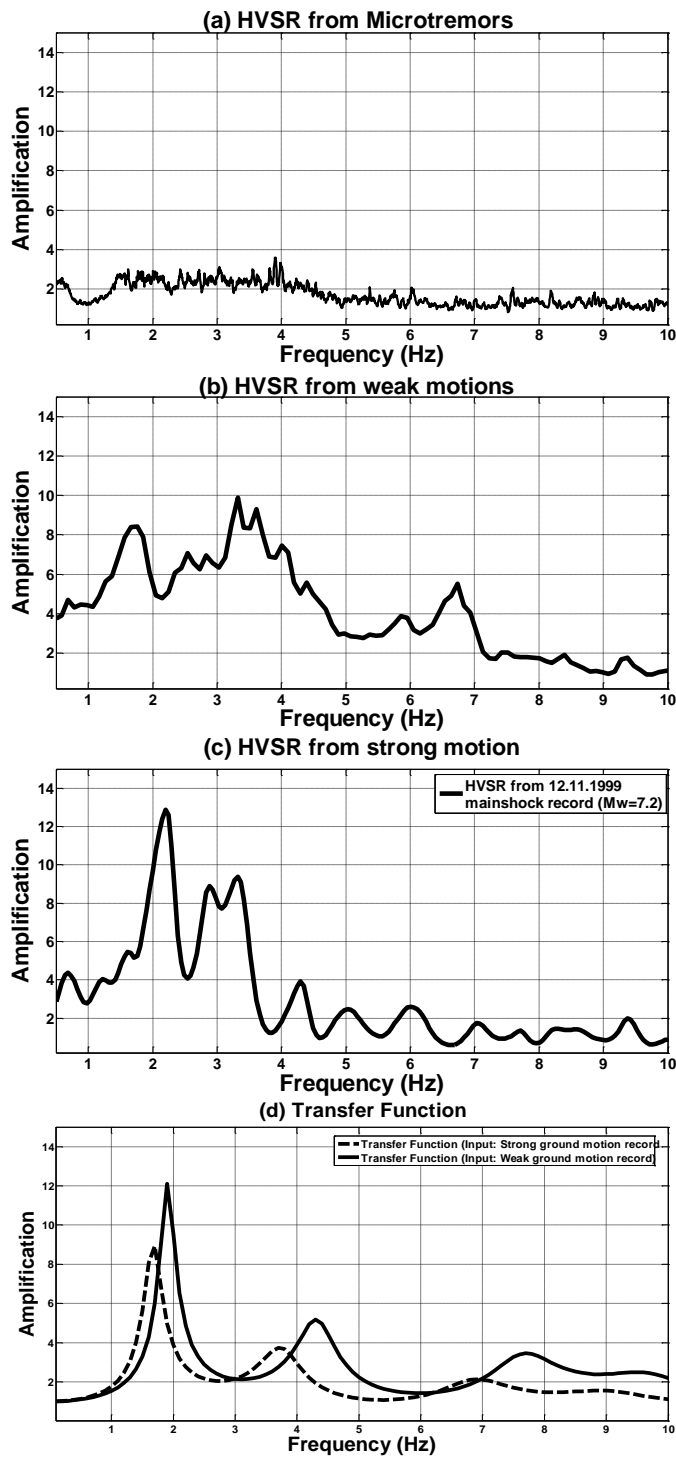


Figure 3.15: Comparison of amplification spectra at Bolu in terms of (a) HVSr from microtremors, (b) HVSr from weak motions, (c) HVSr from 1999 Kocaeli and 1999 Düzce mainshocks, (d) Theoretical transfer functions

CHAPTER 4

SUMMARY AND CONCLUSIONS

4.1 Summary

In this thesis, soil amplification factors and modal frequencies from alternative methods are computed and compared with each other at two different sites located in Northwestern Turkey. The input soil model is obtained in the first part of the study and employed later in the second part.

In the first part of the thesis, microtremor records collected in Düzce and Bolu are interpreted with MMSPAC methodology. In the field work, triangular arrays are utilized with four three-component seismometers to obtain inter-station coherency spectra. Then, starting with an initial S-wave velocity profile, iterative forward fitting is performed until observed and modeled coherency curves match each other. Finally, S-wave velocity profiles are obtained at sites of interest.

In the second part of the study, amplification factors and the corresponding modal frequencies are obtained from empirical HVSR methods as well as 1D theoretical transfer functions. The empirical HVSR method is performed on both microtremor and earthquake data. The earthquake data are categorized into two groups with respect to their PGA values: weak and strong ground motions. The purpose of this categorization is to evaluate potential nonlinearity effects of the soil. The theoretical transfer functions are computed from the 1D shear-velocity profile obtained in Chapter 2.

Alternative methods yielded complementary results suggesting that whenever possible different methods should be used together for reliable S-wave velocity profiles.

4.2 Conclusions

In Chapter 2, following conclusions are drawn during the implementation of the MMSPAC method:

- The use of a multi-mode method allows the S-wave velocity profiles to include the high-frequency energy which otherwise would be missed.
- Use of a small array with even 4 stations is helpful to obtain a reliable velocity model at each site of interest.
- MMSPAC has the advantage of simultaneously resolving the shallow, middle and deeper parts of the soil structure.
- Use of MMSPAC method together with HVSR makes it possible to obtain velocity profiles down to deeper structure.
- Rather than the costly and invasive methods such as drilling, explosions and other seismic methods, MMSPAC solely relies on passive noise measurements. This is important in particular in the urban areas where the invasive methods cannot be easily utilized.

- Other than the initial instrument cost, MMSPAC method is much less expensive and faster than the other techniques.
- It is important to get rid of the extra background noise during measurements for reliable results.

In Chapter 3, comparison of results from alternative techniques in terms of amplification factors and fundamental frequencies yields the following conclusions:

- Empirical estimates of the fundamental frequencies from HVSR method based on microtremors and weak motions are generally consistent. However near-field strong motion data with larger amplitudes could indicate lower fundamental frequency values than those from weak motions and microtremors. This is mostly due to near source effects or nonlinear behavior of the soil under strong ground motions. However, this observation is valid for the lower modes only. For the higher modal frequencies, empirical estimates from HVSR based on different types of data are consistent with each other.
- The amplification ratios obtained with the HVSR method vary depending on the type of data employed to compute the spectral ratios. The strong motion HVSR and weak motion HVSR yield similar results in terms of the amplification factors however the amplitudes are generally underestimated by the microtremor HVSR.
- The amplitudes corresponding to low frequencies obtained from HVSR of strong motion records are larger than the results from other techniques. This is believed to originate mostly from source effects dominant in near-fault strong motion records which cannot be fully eliminated in the HVSR applications. Again, near-field large amplitude strong motion records could indicate nonlinearity with lower amplification ratios when compared to other strong motion records with smaller amplitudes. Thus, even though HVSR based on single strong motion records can be employed to study potential nonlinear effects during a particular event, they are not recommended as reliable estimates of site amplification factors since they dominantly contain active seismic energy as opposed to microtremors and weak motions. Empirical HVSR based on aftershocks or microtremors are thus more stable for estimating site response.
- The microtremor dataset which is used to construct the empirical HVSR curves is also employed in MMSPAC inversions to obtain 1D wave velocity profiles at the sites of interest. The theoretical transfer functions computed using these soil profiles yield estimates of the fundamental and higher mode frequencies that are consistent with the values obtained from other methods. However, due to the inelastic material modeling involved, SHAKE results are naturally dependent on the input base ground motion record. Thus, the amplification factors can vary considerably with the input motion employed. The results of this thesis show that the amplitudes from the theoretical transfer functions with weak motions are consistent with single-record empirical HVSR curves.
- The efficiency of theoretical transfer functions based on 1D soil models in estimating the fundamental frequencies and amplification factors is an interesting observation considering that both stations are located in sedimentary basins with heterogeneous velocity structures.

- Finally, the results are obtained at two soil sites only. Yet the results of this thesis are consistent with several past studies from other regions (e.g.: Lebrun et al., 2004; Massa et al., 2004). Further confirmation of conclusions will require similar case studies at other locations. Such studies will guide the choice of method for future estimation of dynamic properties of soils in earthquake risk assessment studies.

4.3 Future Work and Recommendations

- For future studies, MMSPAC method could be used with higher number of stations per array whenever possible for obtaining more inter-station separations yielding higher accuracy.
- MMSPAC method could be used in deriving not only 1D velocity models but also 2D and 3D heterogeneous basin structures. Such an attempt would require long and dense arrays in both horizontal directions. The author and the supervisor of this thesis are working towards such a study in Erzincan basin.
- For the empirical HVSr, larger number of records could be employed at each station. Different magnitude bins could as well be further categorized to study the nonlinear effects in detail.
- Performance of all methods employed in this thesis relies on the quality of the data used. For both ground motions and microtremors, recording and storing high-quality data is extremely significant in terms of reliable results.
- 1D theoretical transfer functions are used in this thesis. In the future, spectral ratios from 2D or 3D wave propagations could be used to account for theoretical (numerical) amplification phenomena. Such studies would as well include the basin and topography effects in site amplifications.
- While it is recognized it may be difficult to apply alternative methods for modeling site response at all locations of interest, it is recommended that whenever possible, alternative estimates for fundamental frequencies and amplification factors should be assessed.

REFERENCES

- Aki, K. (1957). Space and time spectra of stationary stochastic waves, with special reference to microtremors. *Bull, Earthq. Res. Inst*, Vol **35**, pp 415-456.
- Alexoudi, M., D. Manou, and K. Pitilakis (2008). Seismic Vulnerability Analysis of Waste-Water System: Methodology and Application for Kocaeli and Düzce Earthquakes Based on the Microzonation Study of Düzce, The 14th World Conference on Earthquake Engineering October 12-17, 2008, Beijing, China.
- Ansal, A., A. Kurtuluş, and G. Tönü (2007). Bolu İl Merkezi Sismik Mikrobölgeleme Çalışması, B.Ü. Kandilli Rasathanesi ve Deprem Araştırma Enstitüsü Araştırma Raporu, Bölüm 2.
- Asten M.W. (1976). The use of microseisms in geophysical exploration: PhD Thesis, Macquarie University.
- Asten, M.W., T. Dhu (2002). Enhanced interpretation of microtremor spectral ratios using multimode Rayleigh-wave particle motion computations. In: Griffith, M., Love, D., McBean, P., McDougall, A., Butler, B. (Eds.), Total Risk Management in the Privatized Era. Proceedings of Conference, *Australian Earthquake Engineering Soc.*, Adelaide, Paper 8, pp. 28-1–28-6.
- Asten, M.W., T. Dhu, A. Jones and T. Jones (2003). Comparison of shear velocities measured from microtremor array studies and SCPT data acquired for earthquake site hazard classification in the northern suburbs of Perth W.A., *Proceedings of a Conference of the Australian Earthquake Engineering Soc.*, **12** p., Melbourne.
- Asten, M.W., T. Dhu, and N. Lam (2004). Optimized array design for microtremor array studies applied to site classification; observations, results and future use, Paper 2903, *Conference Proceedings of the 13th World Conference of Earthquake Engineering*, 1-6 Aug 2004, Vancouver, Canada.
- Asten, M.W., and D.M. Boore (2005). Microtremor methods applied to hazard site zonation in the Santa Clara Valley, *Seismological Society of America (SSA)* 27-29 April 2005, Lake Tahoe, Nevada, U.S.
- Asten, M.W. (2005). An assessment of information on the shear-velocity profile at Coyote Creek, San Jose, from SPAC processing of microtremor array data, in Asten, M.W., and Boore, D.M., eds., Blind comparisons of shear-wave velocities at closely spaced sites in San Jose, California, U.S. *Geol. Surv. Open-File Rept.* 2005-1169.
- Asten, M.W., W.R. Stephenson and P. Davenport (2005). Shear-wave velocity profile for Holocene sediments measured from microtremor array studies, SCPT, and seismic refraction, *J. Environ. Eng. Geophys.*, **10**, 235-242.
- Asten, M.W. (2006a). On bias and noise in passive seismic data from finite circular array data processed using SPAC methods, *Geophysics*, **71** (6), V153-V162.
- Başokur, A.T. (2005). Yapı-Yeri İncelemelerinde Makaslama Dalgası Hız Kesitinin ReMi Yöntemi İle Saptanması, Kocaeli Deprem Sempozyumu 2005, 23-25 Mart 2005, Kocaeli.
- Cho, I., T. Tada, and Y. Shinozaki (2006). A generic formulation for microtremor exploration methods using three-component records from a circular array, *Geophysics J. Int.*, **165**, 236–258, doi 10.1111/j.1365-246X.2006.02880.x.

Claproud, M., M.W. Asten and J. Kristek (2011). Evaluation of SWV profile in 2D environments with the spatially averaged coherency microtremor method (SPAC), *Bull. Seism. Soc. Am.*, **101**, 826–847, doi 10.1785/0120090232.

Field, E.H., and K.H. Jacob (1993). The Theoretical Response of Sedimentary Layers to Ambient Seismic Noise, *Geophysical. Res. Lett.*, **20**, 2925–2928.

García-Jerez, A., F. Luzón, and M. Navarro (2008). An alternative method for calculation of Rayleigh and Love wave phase velocities by using three-component records on a single circular array without a central station, *Geophysical. J. Int.*, **173**, 844–858.

Herrmann, R.B., (2001). Computer programs in seismology, An overview of synthetic seismogram computation: Version 3.1: Department of Earth and Planetary Sciences, St. Louis University.

Huang, H., and T. Teng (1999). An Evaluation on H:V Ratio vs. Spectral Ratio for Site-response Estimation Using the 1994 Northridge Earthquake Sequences, *Pure Appl. Geophys.* **156**, 631–649.

Köhler, A., M. Ohrnberger, F. Scherbaum, M. Wathelet, and C. Cornou (2007). Assessing the reliability of the modified three-component spatial autocorrelation technique, *Geophysical. J. Int.*, **168**, 779–796.

Kramer, S.L. (1996). Geotechnical Earthquake Engineering, Prentice Hall, Inc., Upper Saddle River, New Jersey, 653 pp.

Kudo, K., T. Kanno, H. Okada, O. Ozel and M. Erdik (2002). Site-specific issues for strong ground motions during the Kocaeli, Turkey, earthquake of 17 August 1999, as inferred from array observations of microtremors and aftershocks, *Bull. Seismol. Soc. Am.*, **92**, 448–465.

Lachet, C., and P.Y. Bard (1994). Numerical and theoretical investigations on the possibilities and limitations of Nakamura's technique, *J. Phys. Earth*, **42**, 377–397.

Lebrun, B., A.M. Duval, P.Y. Bard, O. Monge, M. Bour, S. Vidal, and H. Fabriol (2004). Seismic microzonation: A comparison between geotechnical and seismological approaches in Pointe-à-Pitre (French West Indies). *Bulletin of Earthquake Engineering*, **2** (1), 27 -50.

Lermo, J., and F. Chavez-Garcia (1993). Site effect evaluation using spectral ratio with only one station. *Bulletin of the Seismological Society of America*, **83** (5), 1,574–1,594.

Louie, J.N. (2001). Faster, Better: Shear-wave velocity to 100 meters depth from refraction microtremor arrays, *Bull. Seism. Soc. Am.*, **91**, 347-364.

Maresca, R., L. Nardone, D. Galluzzo, M. La Rocca and E. Del Pezzo (2006). Application of the SPAC method to Ambient noise Recorded in the Vesuvius Area (Italy). Proc. III Int. Symp. on the Effects of Surface 5 Geology on Seismic Motion, Grenoble, France, August 30 - September 1, 2006, I: 345-350.

Massa, M., G. Feretti, A. Cevasco, L. Isella, and C. Evaa (2004). Analysis of Site Amplification Phenomena: An Application in Ripabottoni for the 2002 Molise, Italy, *Earthquake Spectra*, **20**, No. S1, S107–S118.

Nakamura, Y., (1989). A method for dynamic characteristics estimation of subsurface using microtremor on the ground surface, *Q. Rep. Railway Tech. Res. Inst.*, **30**, 25–30.

- Nazarian, S., and M.R. Desai (1993). Automated surface wave method: Field testing. *Journal of Geotechnical Engineering*, **199**, p. 1094-1111.
- Nogoshi, M., and T. Igarashi (1971). On the amplitude characteristics of microtremor, Part II: *Journal of the Seismological Society of Japan*, **24**, 26–40.
- Okada, H., (2003). The Microtremor Survey Method, *Geophysical Monograph Series*, **12**, SEG, Tulsa.
- Park, C.B., R.D. Miller and J. Xia (1999). Multi-channel analysis of surface waves, *Geophysics*, **64**, 800-808.
- Roberts, J., and M.W. Asten, 2004, Resolving a velocity inversion at the geotechnical scale using the microtremor passive seismic survey method: *Exploration Geophysics*, **35**, 14–18.
- Roberts, J., and M.W. Asten (2007). Further investigation over Quaternary silts using the SPAC and Horizontal to Vertical Spectral Ratio (HVSr) microtremor methods, *Explor. Geophys.*, **38** (3), 175-183.
- Rodriguez, V.H.S., and S. Midorikawa (2002). Applicability of the H/V spectral ratio of microtremors in assessing site effects on seismic motion, *Earthquake Engng Struct. Dyn.*, **31**, 261–279.
- Rosenblad, B., E.M. Rathje, and K.H. Stokoe (2006). Shear Wave Velocity Profiling by the SASW Method at Selected Strong-Motion Stations in Turkey, Project Final Report.
- Rosenblad, B.L. and J. Li (2009). Comparative Study of Refraction Microtremor (ReMi) and Active Source Methods for Developing Low-Frequency Surface Wave Dispersion Curves, *Journal of Environmental and Engineering Geophysics*, in press.
- Saito, M., (1979). Computations of reflectivity and surface wave dispersion curves for layered media, Part I — Sound wave and SH wave: *Butsuri- Tansa*, **32**, 15–26.
- Saito, M., (1988) Compound matrix method for the calculation of spheroidal oscillation of the earth, *Seismological Research Letters*, **59**, 29.
- Schmidt, R.O. (1986). Multiple emitter location and signal parameter estimation. *IEEE Transactions on Antennas and Propagation*, AP-34, 276-280.
- Schnabel, P.B., J. Lysmer, and H.B. Seed (1972). SHAKE: A computer program for earthquake response analysis of horizontally layered sites, Report No UCB/EERC-72/12, *Earthquake Engineering Research Center*, University of California, Berkeley, p. 102.
- Schramm, K., H. Patton, R. Abbott, S. Bilek, A. Pancha and M.W. Asten (2012). Broadband Rayleigh-Wave Dispersion Curve and Shear Wave Velocity Structure for Yucca Flat, Nevada, *Bull. Seism. Soc. Am.* in press.
- Şengör, A.M.C., O. Tuysuz, C. Imren, M. Sakinc, H. Eyidogan, N. Gorur, X. Le Pichon and C. Rangin (2005). The North Anatolian Fault: A new look, *Annu. Rev. Earth Planet. Sci.* **33**:37–112, doi 10.1146/annurev.earth.32.101802.120415.
- Stephenson W.J. and J.K. Odum (2011). Application of the Spatial-autocorrelation Microtremor-array Method for Characterizing S-wave Velocity in the Upper 300m of Salt Lake Valley, Utah, *Advances in Near-Surface Seismology and Ground-Penetrating Radar* By Richard D Miller, Jr. Jr, John H. Bradford, Klaus Holliger, *Society of Exploration Geophysicists*, Rebecca B. Latimer

Stephenson, W., S. Hartzell, A. Frankel, M.W. Asten, D. Carver and W. Kim (2009). Site characterization for urban seismic hazards in lower Manhattan, New York City, from microtremor array analysis, *Geophys. Res. Lett.*, **36**, L03301, doi 10.1029/2008GL036444.

Suzuki, T., Y. Adachi, and M. Tanaka (1995). Application of Microtremor Measurements to the Estimation of Earthquake Ground Motions in Kushiro City during the Kushiro-Oki Earthquake of 15 January 1993, *Earthquake Eng. Struct. Dyn.*, **24**, 595–613.

Şimsek, O and S. Dalgıç (1997). Düzce Ovası killerinin konsolidasyon özellikleri ve jeolojik evrim ile ilişkisi, *Geological Bulletin of Turkey*, **V.40**, No 2.

Tatar, Y. (2003). Bolu İl Gelişme Planı Çevre ve Mekansal Yapı Raporu, Abant İzzet Baysal Üniversitesi

Toksoz, M. N. and R. T. Lacoss (1968). Microseisms: mode structures and sources, *Science* **159**, 872-873.

Tokgöz E. (2002). Bolu ve Yakın Çevresinde Mikrotremor Verileri ile Yer Etkisinin İncelenmesi Yüksek Lisans Tezi, Jeofizik Müh. Bölümü, Ankara Üniversitesi, Ankara

Utkucu, M., S.S. Nalbant, J. McCloskey, S. Steacy, and O. Alptekin (2003). Slip distribution and stress changes associated with the 1999 November 12, Duzce (Turkey) earthquake (Mw = 7.1), *Geophys. J. Int.* **153**, 229–241.

Wathelet, M., D. Jongmans, and M. Ohrnberger (2005). Direct Inversion of Spatial Autocorrelation Curves with the Neighborhood Algorithm. *Bulletin of the Seismological Society of America*, **95**, 1787-1800

Wen K.L., I. A. Beresnev and Y.T. Yeh (1994). Nonlinear soil amplification inferred from downhole strong seismic motion data, *Geophysical Research Letters*, **21**, 625–2628.

Yamanaka, H., M. Kato, M. Hashimoto, U. Gulerce, R. Iyisan, A. Ansal (2002). Microtremor and earthquake observations in Adapazarı and Düzce, Turkey, for estimations of site amplifications, *Proceedings Assessment of Seismic Local-Site Effects at Plural Test Sites, Ministry of Education, Science, Sports and Culture, Research Grant No: 11694134, Japan, March 2002, 129-136.*

Yılmaz et al. (2006). Compilation of Data Base for The National Strong-Motion Seismograph Network in Turkey - Report on Seismic and Geotechnical Investigations: Earthquake Engineering Research Center of Middle East Technical University and Earthquake Research Department of The General Directorate of Disaster Affairs, TÜBİTAK Research Project, No. 105G016, Turkey.

Yılmaz, Ö., E. Savaşkan, S. Bakır, T. Yılmaz, M. Eser, S. Akkar, B. Tüzel, Y. İravul, Ö. Özmen, Z. Denizlioğlu, A. Alkan and M. Gürbüz (2008). Shallow seismic and geotechnical site surveys at the Turkish national grid for strong-motion seismograph stations, 14th World Conference on Earthquake Engineering, Pekin, China, No. 03-03-0014.

Yılmaz, Ö., M. Eser, A. Sandıkkaya, S. Akkar, S. Bakır and T. Yılmaz (2008b). Comparison of shear-wave velocity-depth profiles from downhole and surface seismic experiments, 14th World Conference on Earthquake Engineering, Pekin, China.

Zywicki, D.J. (1999). Advanced Signal Processing Methods Applied To Engineering Analysis of Seismic Surface Waves, *Georgia Institute of Technology*, PhD Thesis, 227p, Georgia.

Web References:

Web Page of Strong Ground Motion Database of Turkey: <http://daphne.deprem.gov.tr>

Web Page of General Directorate of Mineral Research and Exploration: www.mta.gov.tr

APPENDIX A

ADDITIONAL CASE STUDIES

In addition to the MMSPAC analyses performed at Düzce and Bolu, raw SPAC data from other locations in the world are analyzed to gain further insight to the method. The data presented herein is obtained from field tests performed in Austria as a part of the EU-SERIES project in 2009. These arrays are constructed on a soccer ground in Wien, Austria. The tests are performed during daytime but on Sunday to eliminate noise. Three vertical geophones are used and a small radius of 7m is employed.

Results of MMSPAC analyses performed on these data are presented herein.

A.1 Wien 1 Data

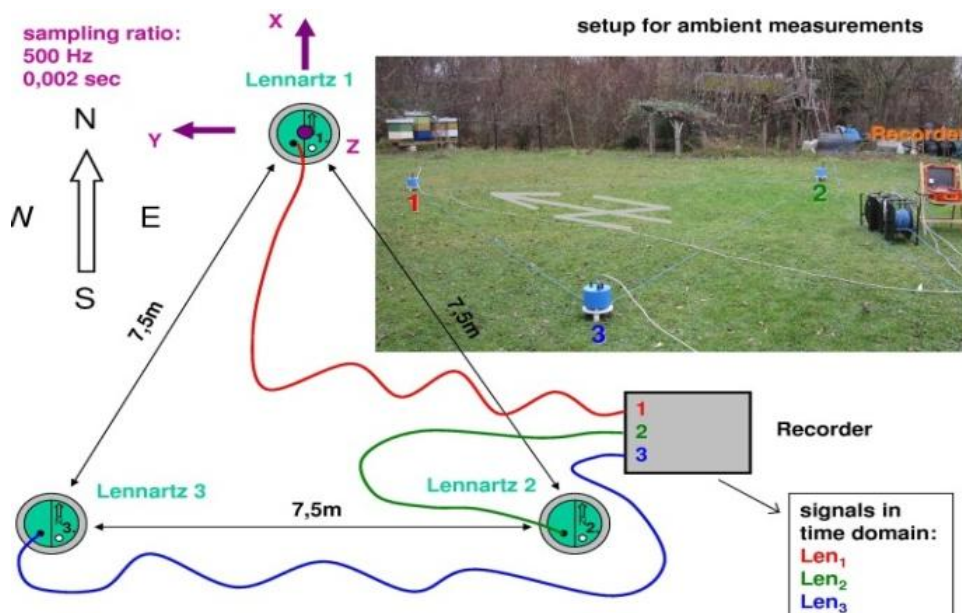


Figure A.1: Sketch map of array measurements

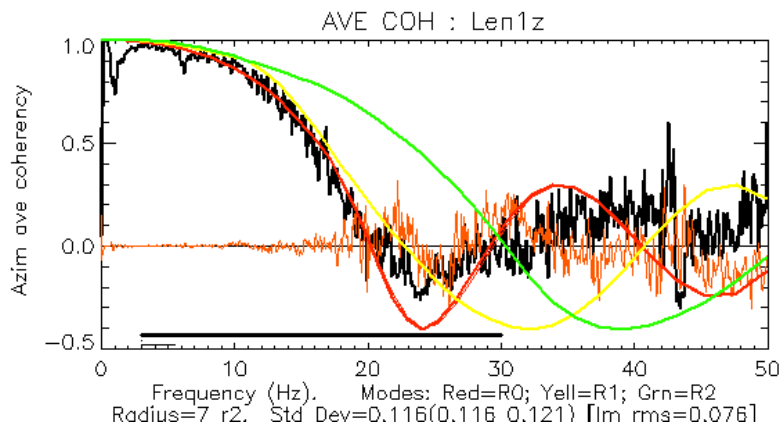


Figure A.2: SPAC coherency curve at Wien 1

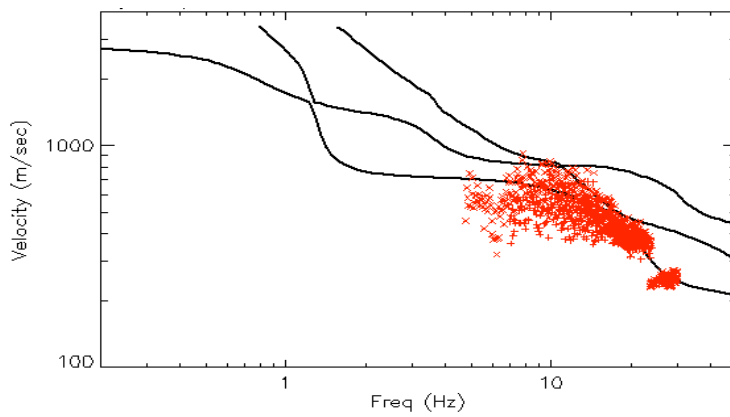


Figure A.3: Dispersion curve at Wien 1 (Black curves indicate theoretical dispersion curves whereas the red dots indicate observed dispersion)

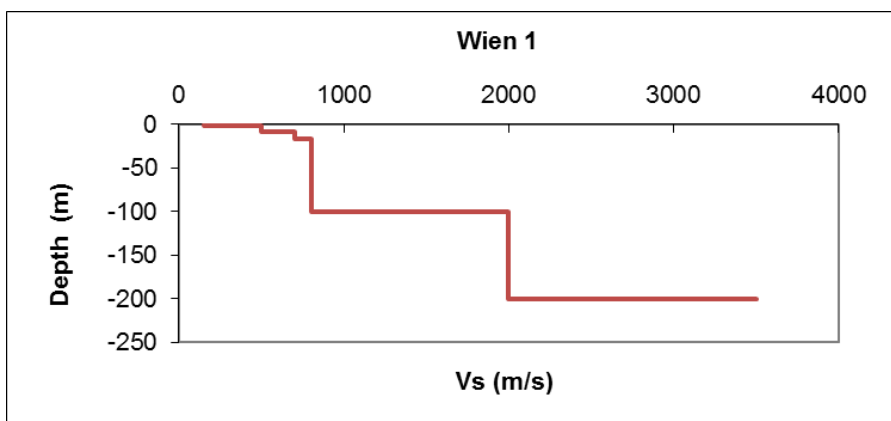


Figure A.4: S-wave velocity profile at Wien 1 (Radius: 10m)

Table A.1: Layered-earth model at Wien 1 (Radius: 7m)

Layer Number	Thickness (m)	Vp (m/s)	Vs (m/s)	Rho (t/m ³)
1	1	450	150	1.8
2	2	600	200	1.8
3	2	900	300	2.0
4	8	1750	550	2.0
5	16	2400	800	2.20
6	25	3000	1000	2.20
7	250	3500	2000	2.20
8	Infinite	6040	3490	2.4

A.2 Wien 2 Data

The orange triangles displayed in Figure A.4 show the planned sensor positions whereas the red triangles depict the final test positions (i.e. the correct ones). Radii are 10m, 20m, 40m, 80m and 160m. In addition, to single site solutions, multiple interpretations are performed with 40m, 80m and 160m arrays.

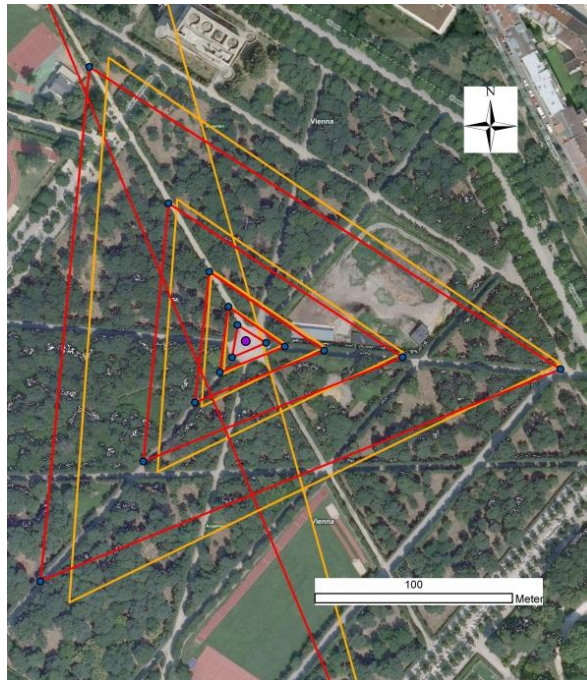


Figure A.5: Sketch map of arrays at Wien

A.2.1 Results of the radius 10m

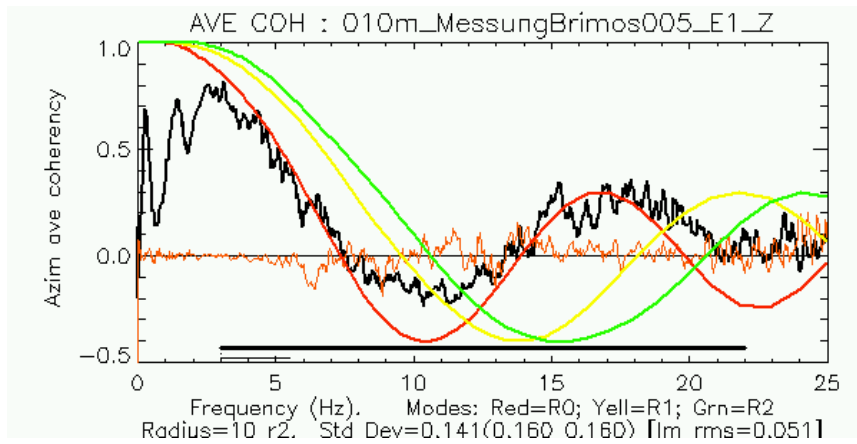


Figure A.6: SPAC coherency curve at Wien 2 for radius 10m

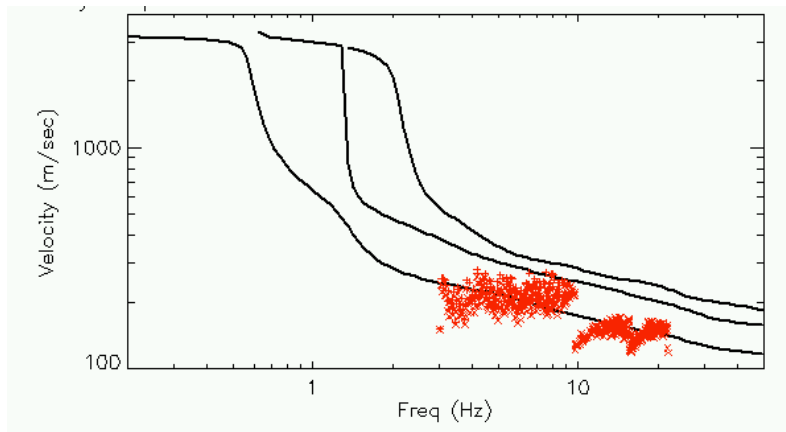


Figure A.7: Dispersion curve at Wien 2 for radius 10m (Black curves indicate theoretical dispersion curves whereas the red dots indicate observed dispersion)

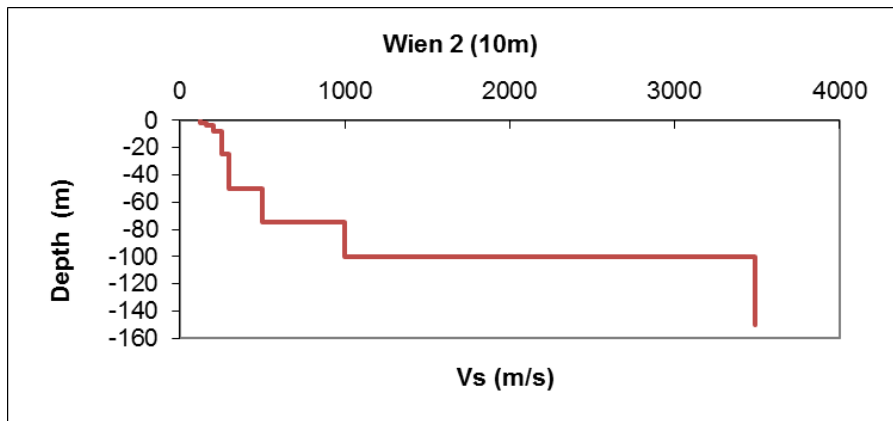


Figure A.8: S-wave velocity profile at Wien 2 (Radius: 10m)

Table A.2: Layered-earth model at Wien 2 (Radius: 10m)

Layer Number	Thickness (m)	Vp (m/s)	Vs (m/s)	Rho (t/m ³)
1	2	450	120	1.78
2	4	500	160	2.0
3	8	600	200	2.0
4	25	750	250	2.14
5	50	900	300	2.14
6	75	1500	500	2.14
7	100	2940	1000	2.39
8	Infinite	6040	3490	2.8

A.2.2 Results of the radius 20m

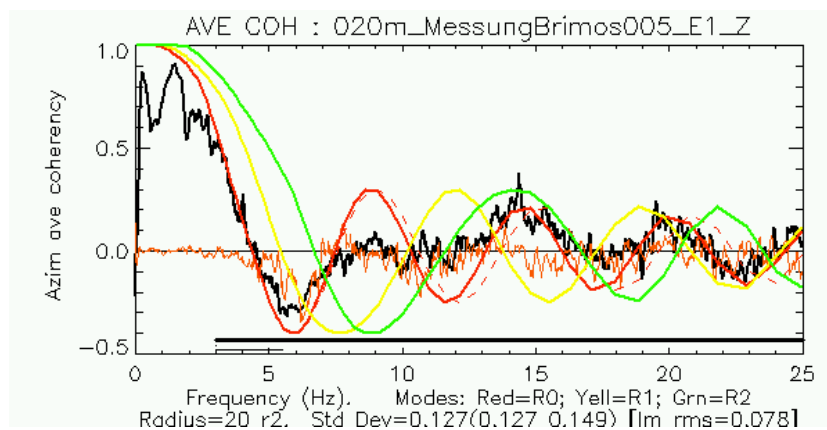


Figure A.9: SPAC spectrum at Wien 2 for radius 20m

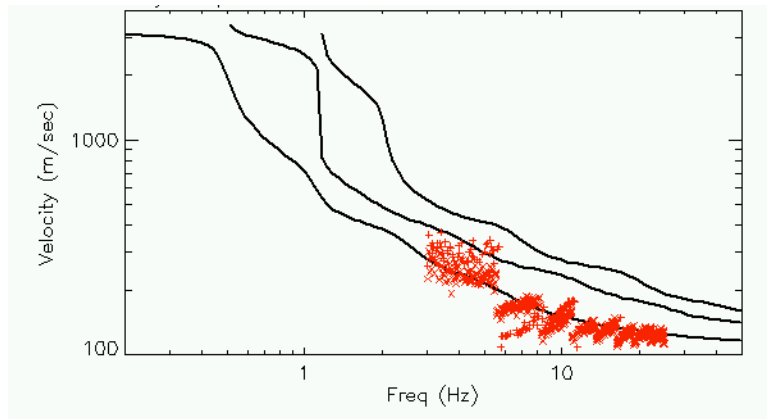


Figure A.10: Dispersion curve at Wien 2 for radius 20m (Black curves indicate theoretical dispersion curves whereas the red dots indicate observed dispersion)

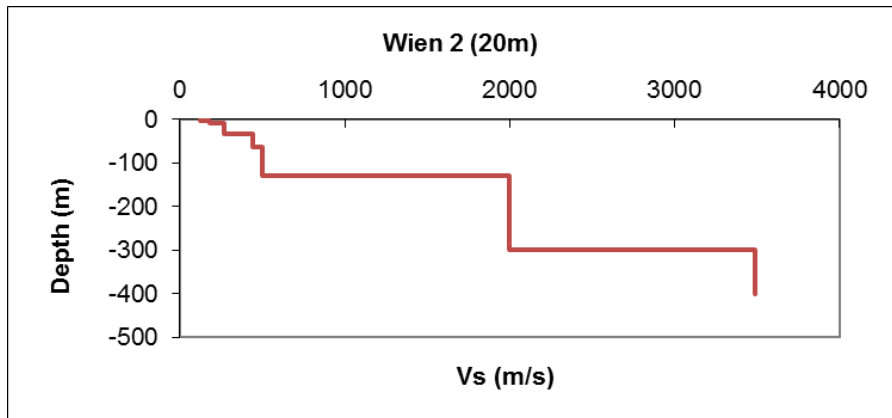


Figure A.11: S-wave velocity profile at Wien 2 for radius 20m

Table A.3: Layered-earth model at Wien 2 (Radius: 20m)

Layer Number	Thickness (m)	Vp (m/s)	Vs (m/s) (m/s)	Rho (t/m ³)
1	2	450	120	1.78
2	4	500	140	2.0
3	8	600	180	2.0
4	32	800	265	2.14
5	64	1500	440	2.14
6	128	200	500	2.14
7	300	2940	2000	2.39
8	Infinite	6040	3490	2.8

A.2.3 Results of the radius 40m

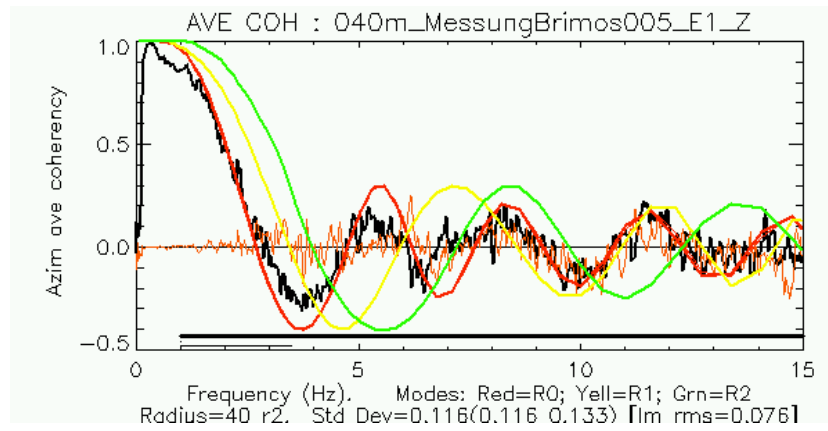


Figure A.12: SPAC spectrum at Wien 2 for radius 40m

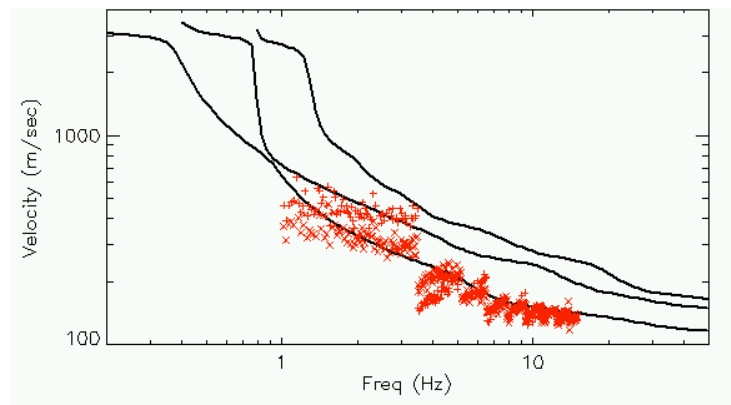


Figure A.13: Dispersion curve at Wien 2 for radius 40m

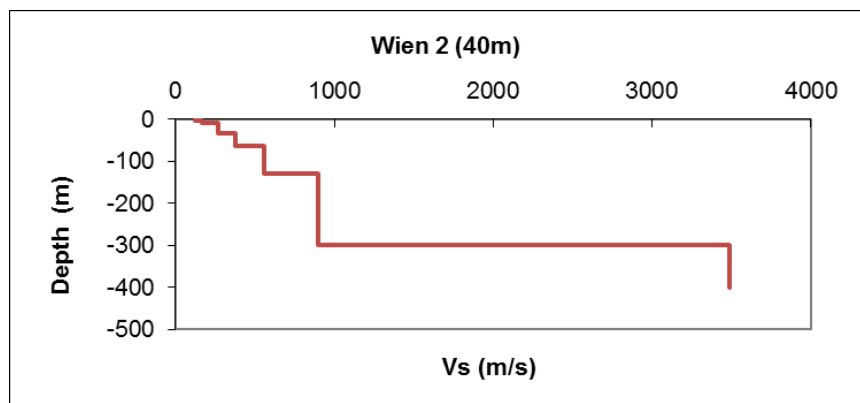


Figure A.14: S-wave velocity profile at Wien 2 for radius 40m

Table A.4: Layered-earth model at Wien 2 (Radius: 40m)

Layer Number	Thickness (m)	Vp (m/s)	Vs (m/s)	Rho (t/m ³)
1	2	450	120	1.78
2	4	500	150	2.0
3	8	600	170	2.0
4	32	800	270	2.14
5	64	1200	380	2.14
6	128	1800	560	2.14
7	300	2940	900	2.39
8	Infinite	6040	3490	2.8

A.2.4 Results of the radius 80m

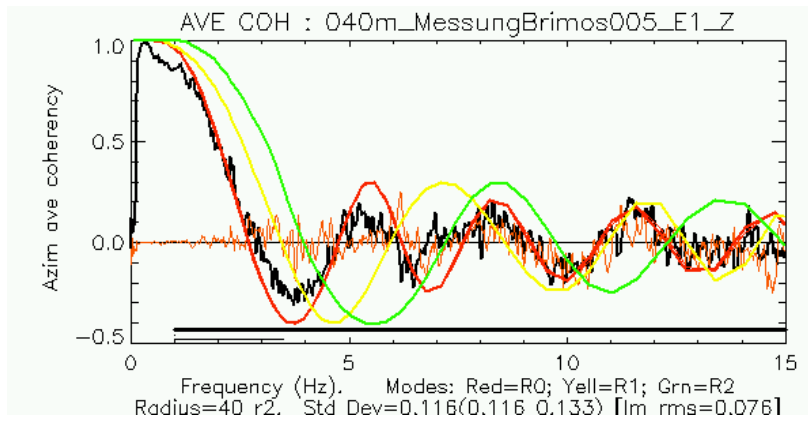


Figure A.15: SPAC spectrum at Wien 2 for radius 80m

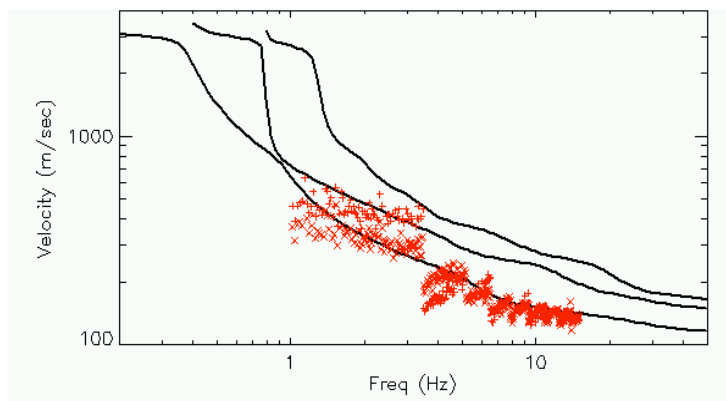


Figure A.16: Dispersion curve at Wien 2 for radius 80m (Black curves indicate theoretical dispersion curves whereas the red dots indicate observed dispersion)

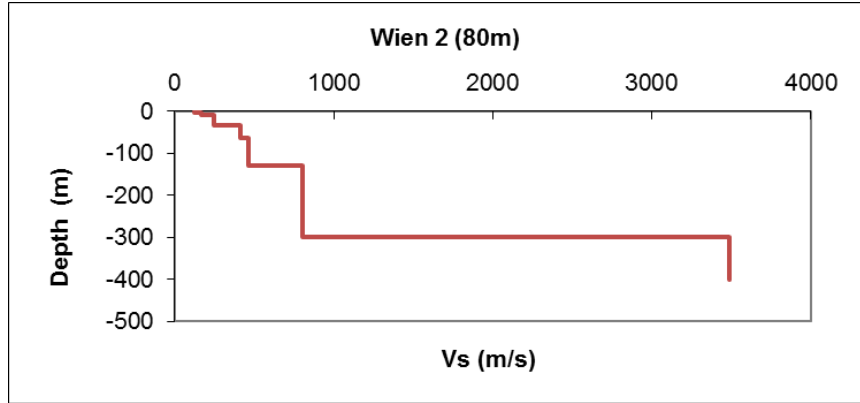


Figure A.17: S-wave velocity profile at Wien 2 for radius 80m

Table A.5: Layered-earth model at Wien 2 (Radius: 80m)

Layer Number	Thickness (m)	Vp (m/s)	Vs (m/s) (m/s)	Rho (t/m ³)
1	2	450	120	1.78
2	4	500	140	2.0
3	8	600	165	2.0
4	32	800	245	2.14
5	64	1200	410	2.14
6	128	1400	465	2.14
7	300	2940	800	2.39
8	Infinite	6040	3490	2.8

A.2.5 Results of the radius 160m

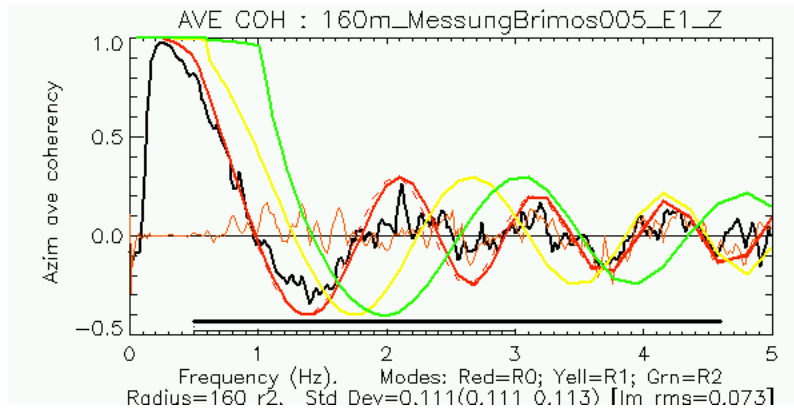


Figure A.18: SPAC spectrum at Wien 2 for radius 160m

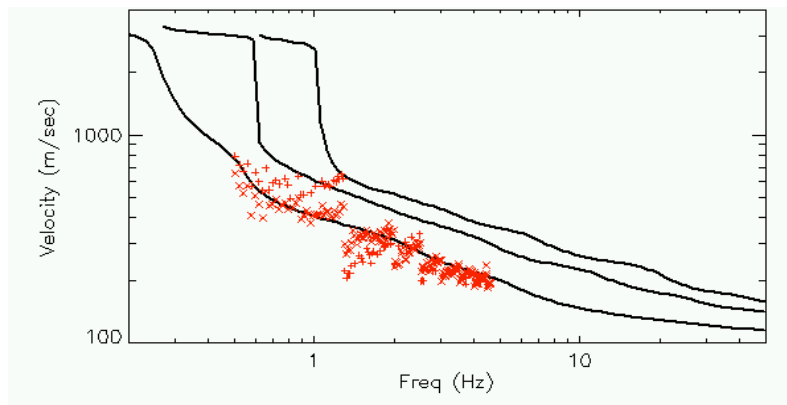


Figure A.19: Dispersion curve at Wien 2 for radius 160m(Black curves indicate theoretical dispersion curves whereas the red dots indicate observed dispersion)

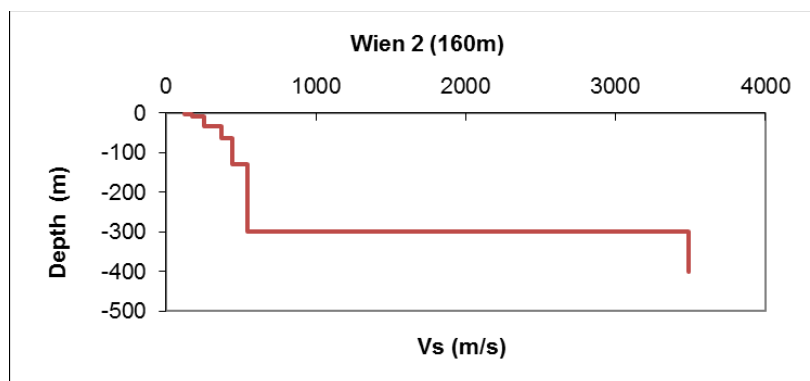


Figure A.20: S-wave velocity profile at Wien 2 for radius 160m

Table A.6: Layered-earth model at Wien 2 (Radius: 160m)

Layer Number	Thickness (m)	Vp (m/s)	Vs (m/s)	Rho (t/m ³)
1	2	400	120	1.78
2	4	450	140	2.0
3	8	600	175	2.0
4	32	800	250	2.14
5	64	1200	370	2.14
6	128	1400	440	2.14
7	300	2940	545	2.39
8	Infinite	6040	3490	2.8

A.2.6 Results of the multiple solution (Radii 40m-80m and 160m)

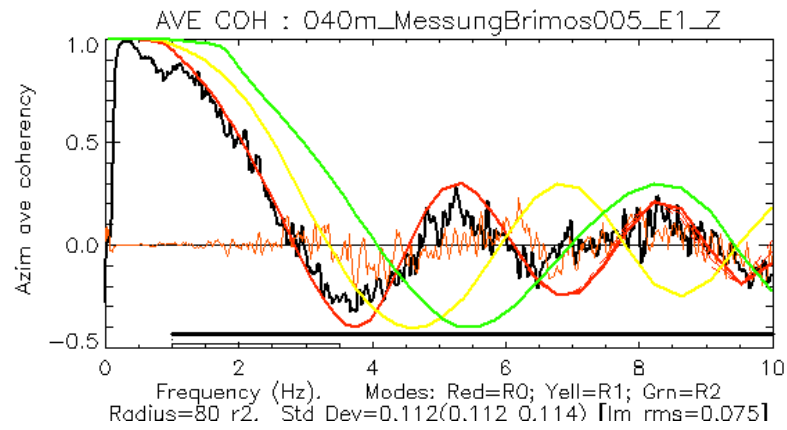


Figure A.21: SPAC spectrum at Wien 2 for multiple solutions

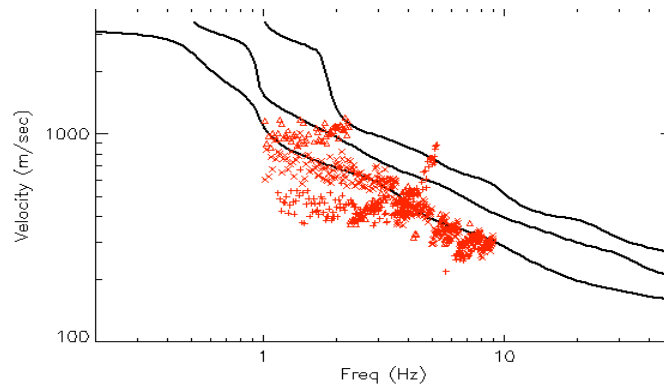


Figure A.22: Dispersion curve at Wien 2 for multiple solutions (Black curves indicate theoretical dispersion curves whereas the red dots indicate observed dispersion)

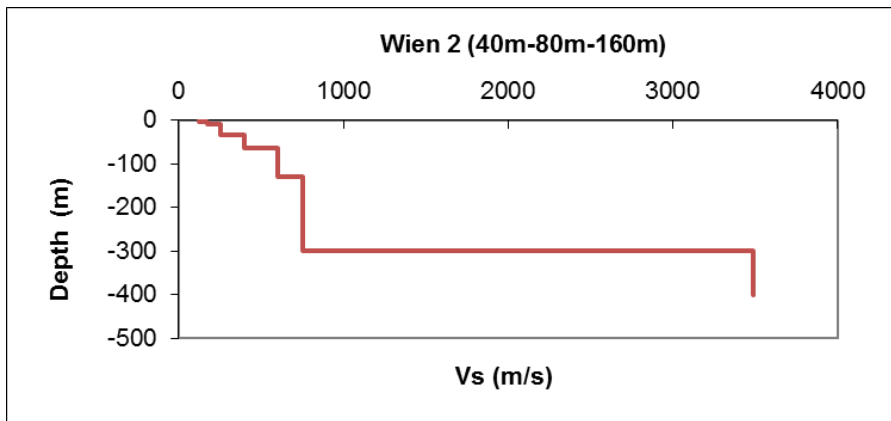


Figure A.23: S-wave velocity profile at Wien 2 for multiple solutions

Table A.7: Layered-earth model at Wien 2 (multiple solutions)

Layer Number	Thickness (m)	Vp (m/s)	Vs (m/s) (m/s)	Rho (t/m ³)
1	2	400	120	1.78
2	4	450	140	2.0
3	8	600	175	2.0
4	32	800	250	2.14
5	64	1200	400	2.14
6	128	1400	600	2.14
7	300	2940	750	2.39
8	Infinite	6040	3490	2.8

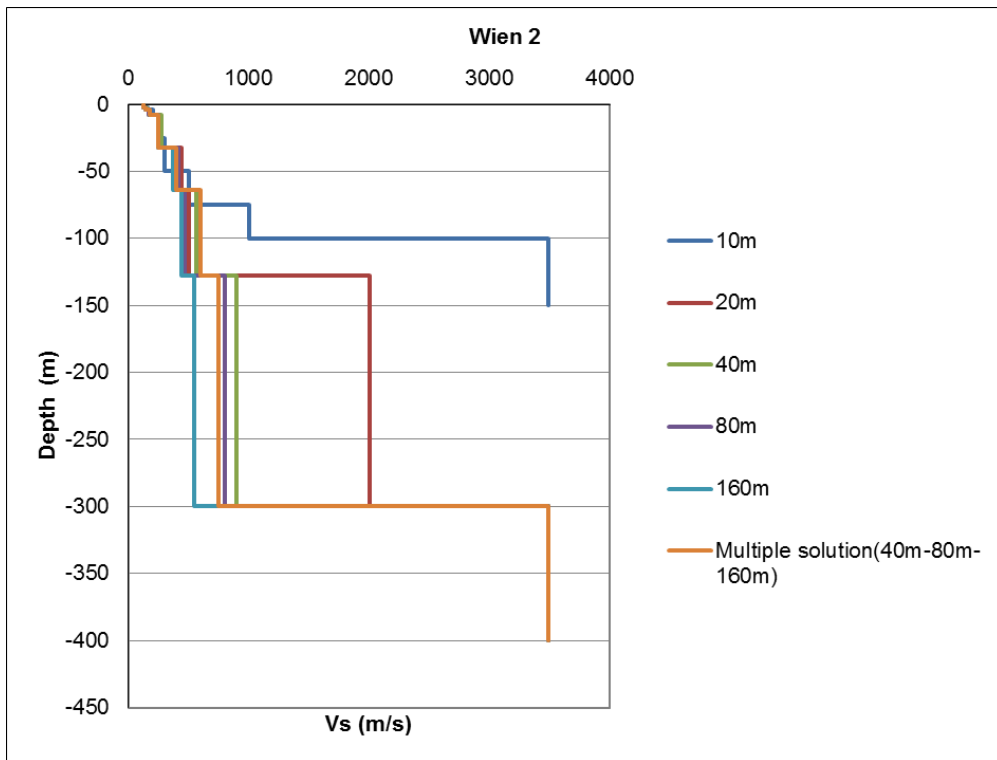


Figure A.24: S-wave velocity profile at Wien 2 for multiple solution